Robust Adaptive Control for Fully Actuated Hexa-Rotors Without Precise Knowledge of Rotor Poses

Alejandro Flore, Andres Montes de Oca, Jean-Baptiste Mouret, Thibaut Raharijaona, Franck Ruffier, Gerardo Flores

▶ **To cite this version:**

Alejandro Flore, Andres Montes de Oca, Jean-Baptiste Mouret, Thibaut Raharijaona, Franck Ruffier, et al.. Robust Adaptive Control for Fully Actuated Hexa-Rotors Without Precise Knowledge of Rotor Poses. International Journal of Robust and Nonlinear Control, 2026, pp.1-21. ⟨10.1002/rnc.70418⟩. ⟨hal-05543267⟩

HAL Id: hal-05543267

https://hal.science/hal-05543267v1

Submitted on 9 Mar 2026

HAL is a multi-disciplinary open access archive for the deposit and dissemination of scientific research documents, whether they are published or not. The documents may come from teaching and research institutions in France or abroad, or from public or private research centers.

L'archive ouverte pluridisciplinaire **HAL**, est destinée au dépôt et à la diffusion de documents scientifiques de niveau recherche, publiés ou non, émanant des établissements d'enseignement et de recherche français ou étrangers, des laboratoires publics ou privés.

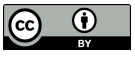

Distributed under a Creative Commons CC BY 4.0 - Attribution - International License

Robust Adaptive Control for Fully Actuated Hexa-Rotors Without Precise Knowledge of Rotor Poses

Alejandro Flores[1] | Andres Montes de Oca[2] | Jean-Baptiste Mouret[3] | Thibaut Raharijaona[4] | Franck Ruffier[5,6] | Gerardo Flores[7]

[1]Center of Research in Mathematics (CIMAT), Guanajuato, Mexico | [2]Center of Applied Physics and Advanced Technology, National Autonomous University of Mexico (UNAM), Campus Juriquilla, Queretaro, Mexico | [3]CNRS INRIA, Université de Lorraine, Nancy, France | [4]Arts et Metiers Institute of Technology, LCFC, Université de Lorraine, Metz, France | [5]Aix Marseille Univ, CNRS, ISM, Marseille, France | [6]ENSTA, Institut Polytechnique de Paris, CNRS, Robex Team, Lab-STICC, Brest, France | [7]RAPTOR Lab, School of Engineering, College of Arts and Sciences, Texas A&M International University, Laredo, Texas, USA

Correspondence: Gerardo Flores (gerardo.flores@tamiu.edu)

Keywords: adaptive control | hexa-rotor full actuation | parameter uncertainties | robust control

ABSTRACT

The control of fully actuated hexa-rotors is highly dependent on their physical parameters, especially those describing the rotors' positions and orientations. Uncertainties in these parameters significantly affect the performance of classical control approaches, particularly in small drones, where manufacturing tolerances amplify these uncertainties. To address this challenge, we propose a novel adaptive and robust control strategy that compensates for parameter uncertainties and external disturbances without requiring precise prior knowledge of the rotor poses. Unlike existing methods, our approach explicitly incorporates motor dynamics into the control design, resulting in a more realistic and implementable framework. Using Lyapunov-based stability analysis, we demonstrate the global asymptotic stability of the proposed control system under parameter uncertainties and disturbances. Extensive simulations validate the efficacy of our method, showcasing superior tracking performance and robustness compared to conventional controllers. This work represents a significant step toward enabling fully actuated multi-rotor UAVs to perform in real-world scenarios with uncertain and dynamic environments.

1 | Introduction

Multi-rotor unmanned aerial vehicles (UAVs) have been scaled down to a few centimeters and a few dozen grams. For instance, the Crazyflie [1] is a nine cm^2 research quadrotor weighing less than 30 g. With their small size, such miniature quadrotors are promising flying platforms for indoor operations, from exploring buildings [2] to getting data in more cave-like spaces [3, 4]. Such small quadrotors exist because they have no moving parts except the four electric motors. This simplicity comes, however, at a cost: since they can only generate four coaxial forces while they need to control six axes, they are underactuated [5]. In concrete terms, quadrotors must tilt their body to perform the translational motion, whereas a fully actuated UAV could track any 6-D pose, including translating without body tilting. The unwanted rotations of an underactuated UAV make it difficult to reject linear perturbations because the UAV needs first to tilt, then move, and then stabilize its rotational velocity; similarly, they make it hard to land precisely because any translation to adjust the position induces some attitude changes. In addition, these rotations in pitch and roll have to be compensated for by optical sensors. For instance, sensors and cameras are typically stabilized using an additional motor (such as a gimbal) to cancel for the rotational flow [6], or the optic flow magnitude is derotated using a derotation process that is not easy to synchronize with the current optic flow measurement [7].

Abbreviation: UAV, unmanned aerial vehicle.

1.1 | Related Work

One of the difficulties in controlling conventional multi-rotors is their inherent property of being an underactuated system, [8]. The latter means that these conventional multi-rotors have more degrees of freedom than control inputs [9]. Several efforts were conducted in the last decade by the UAV and robotics community to alleviate such complexity, see for instance [10, 11]. For that aim, the researchers have proposed some fully actuated multi-rotor platforms [12–14]. However, usually, this approach results in adding extra motors [15], provoking an increment in the weight and size of the aerial robot. In recent years, the robotics, UAV, and control communities have been interested in solving the above problem by proposing fixed-tilted multi-rotors so that the motors can generate both vertical and horizontal forces without adding extra motors [12, 16–19]. These UAVs are less energy-efficient than conventional multi-rotors, but they keep the mechanical design simple and can, therefore, be scaled in size.

Among hexa-rotor platforms, several studies aim to enhance control performance under uncertainties and disturbances. For instance, [20] introduces two architectures: a model reference adaptive controller with a command governor and a dynamic control allocator, evaluated under actuator faults and structured/unstructured uncertainties. Similarly, [21] combines super-twisting observers with nonlinear predictive control for a thrust-vectoring design. Fault-tolerant control is further explored in [22], which employs adaptive backstepping techniques for attitude stabilization under motor failures.

State of the art related to fully actuated hexa-rotors shows that some works have focused on the modeling and control problem [23]. For instance, the control allocation problem is addressed in [24], presenting a methodology for analysis, control allocation, and design of a fully actuated hexa-rotor. Also, in [25], the authors propose a force decomposition to address the control allocation problem of a hexa-rotor with tilted thrusters. It is designed to perform dexterous interaction with structures. Besides, the influence of tilted angles in motors in the hexa-rotor dynamics is relevant as it is investigated in [26], where it studied the fully actuated hexa-rotor's maneuverability by varying the tilting angles. Furthermore, several control techniques to stabilize hexa-rotors have been investigated, such as [16], where an exact feedback linearization and decoupling control law was implemented for stabilization. On the other hand, in [27, 28] it is presented as a hexa-rotor capable of achieving full actuation through one additional motor that tilts all propellers. The stabilization is achieved with a geometric controller. Sliding mode controllers (SMC) are also investigated as in [29] develops an observer-based adaptive SMC for trajectory tracking while carrying a suspended payload, using a high-gain observer to estimate unmeasured states. Another control approach is presented in [30] through a modified Robust Integral of the Sign of Error (RISE) controller that ensures robustness under thrust saturation. Similarly, [31] implements a nonlinear impedance control with force observers for compliant contact interaction. Reference [32] investigates control architectures ensuring both position tracking and attitude regulation by exploiting system flatness and hierarchical control. Reference [33] presents a discrete-time robust controller ensuring trajectory tracking despite model and external disturbances. Also, some visual techniques have been applied to this kind of aerial robot, as in [34]. Practical applications are highlighted in [35], where cascaded PID controllers manage five DOFs in an agricultural tilt-rotor hexa-rotor. Load handling and aerial interaction are addressed in [36] through a layered nonlinear controller for coordinated payload-UAV control. We summarize the most recent and relevant research strongly related to our work in Table 1.

There is considerable flexibility in tolerating mechanical construction variations, particularly in large hexa-rotors. However, achieving precise orientation and positioning of the propellers to minimize uncertainties remains a significant challenge. Recent advancements, such as those presented in [44], have proposed adaptive control solutions to address these issues. Additionally, alternative approaches have been developed, as demonstrated in [45] and [46], where the authors employ Legendre polynomials to design adaptive controllers for uncertain nonlinear systems. While these methods show promise in handling system uncertainties, their adaptation to the specific case of small, fully actuated hexa-rotors poses challenges, as even minimal mechanical tolerances on the order of a few millimeters in rotor positioning can significantly amplify uncertainties in orientation and control. This underscores the urgent need for robust and adaptive control strategies specifically designed to manage the inherent variations in system parameters and external disturbances in such systems.

Complementing the aforementioned contributions to the control of specific platforms, other works explore foundational or supporting aspects. On the modeling and control framework side, [47] proposes a ROS2-PX4-based system enabling decoupled translational and rotational motions in fully actuated hexa-rotors. Reference [13] studies ground effect dynamics across various rotor tilting configurations, and [48] addresses UAV design optimization using hybrid surrogate-based methods to efficiently navigate discrete and continuous parameter spaces.

1.2 | Contribution

Model uncertainties and unknown external disturbances remain critical challenges in the control of small UAVs, particularly in fully actuated multi-rotor systems. While various robust control strategies have been proposed to handle exogenous disturbances, their effectiveness often depends on precise knowledge of the UAV's actuation geometry and actuator dynamics. In practice, even small deviations in rotor orientations or motor parameters, common in compact aerial platforms, can lead to significant performance degradation. Therefore, addressing both types of uncertainties simultaneously is essential for achieving reliable deployment in real-world applications.

In this work, we propose a nonlinear adaptive control framework for a fully actuated hexa-rotor platform, as shown in Figure 1, that explicitly accounts for both modeling uncertainty and actuator-level variability. The core novelty lies in its ability to stabilize the system without requiring exact knowledge of the rotor tilting angles or motor parameters. The control strategy consists of two main components:

TABLE 1 | Relevant state of the art related to fully actuated hexa-rotors.

	Literature	Parameter uncertainty	Robust against disturbances	Stability achieved	Control allocation	Method
1	Our research	✓	✓	Global exponential in attitude and position	✓	Robust and adaptive nonlinear control
2	[37]	✓	✓	None demonstrated	×	Integral sliding mode control
3	[38]	×	×	None demonstrated	×	Feedback linearization and explicit reference governor
4	[39]	×	✓	Asymptotic in attitude and position	×	Super-twisting observer-based sliding mode control
5	[40]	×	×	None demonstrated	×	Observer-based wrench/impedance control
6	[41]	✓	✓	None demonstrated	×	Adaptive super-twisting control
7	[42]	×	×	None demonstrated	×	Nonlinear model predictive control
8	[43]	✓	✓	None demonstrated	✓	Nonlinear model predictive control
9	[29]	×	✓	Finite-time stability	✓	Observer-based adaptive sliding mode controller
10	[30]	×	✓	Local asymptotical stability	×	Satured robust controller
12	[32]	×	✓	None demonstrated	×	Hierarchical controller
15	[36]	×	✓	None demonstrated	✓	PID controller

- A *robust nonlinear controller* that computes the virtual force and torque inputs required to track a desired trajectory, assuming full actuation. This controller ensures global asymptotic convergence of the position and attitude errors, and is robust to external disturbances.
- An *adaptive allocation mechanism* that maps the virtual control inputs to actual motor commands without needing parameter identification. This stage incorporates the full electromechanical dynamics of the motors and relies only on the known sign structure of the actuation configuration. The adaptation law ensures tracking of the desired control signals while compensating for uncertainties in the actuation matrix and motor dynamics.

Unlike existing works that assume calibrated or fixed actuation geometries, our approach is inherently robust to structural variations in the rotor orientations, enabling the use of interchangeable or reconfigurable configurations. This feature is especially relevant for platforms where the tilting angles vary slightly due to manufacturing tolerances or modular design.

Overall, the proposed control strategy provides a unified and implementable solution that combines theoretical guarantees with practical robustness, enabling reliable operation of fully actuated UAVs in the presence of both geometric and dynamic uncertainties.

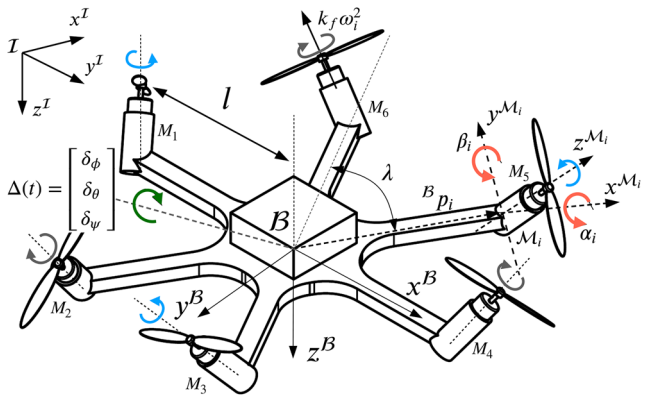

FIGURE 1 | Hexa-rotor design illustration. Each motor (M_i) has fixed tilt angles (α_i, β_i), which rotations are described with orange arrows. Three motors have clockwise rotation shown with gray arrows, and the other three motors have counterclockwise rotation depicted by clear blue arrows. An additional angle λ defines the angular distance between hexa-rotor arms. With this design, it is possible to partially decouple the position and attitude dynamics presented in conventional underactuated multi-rotors. Besides, the hexa-rotor is prone to external disturbances $\Delta(t)$.

1.3 | Content

Section 2 describes the hexa-rotor system and its mathematical model and poses the problem statement. Section 3 presents the two-step control algorithm, summarized in two main theorems that use the matrix sign decomposition. In Section 4, we present the simulations of our control algorithm and some comparisons to verify its effectiveness. Finally, Section 5 provides some conclusions and further investigation on the subject of hexa-rotor control.

2 | The Hexa-Rotor Mathematical Modeling and the Control Problem

This section introduces the design of the fully actuated hexa-rotor configuration. Then, the corresponding mathematical model, considering the six degrees of freedom (6-DOF), is developed. Once the modeling is given, we pose the control problem for stabilizing the fully actuated hexa-rotor.

2.1 | The Fully Actuated Hexa-Rotor Configuration

Let us consider the conventional coplanar hexa-rotor configuration for a while. Like the rest of conventional multi-rotors, the coplanar hexa-rotor configuration is an underactuated system, which causes its attitude to change to achieve $x-y$ displacements. The latter is undesirable for particular UAV applications that require $x-y$ displacements without changing the UAV's attitude. To cope with this, it is possible to strategically arrange the six motors so that the hexa-rotor achieves full actuation. With that aim, and as it can be seen in Figure 2a, motors are rotated with angles (α, β), where $\alpha = \{\alpha_1, \ ..., \ \alpha_6\}$, $\beta = \{\beta_1, \ ..., \ \beta_6\}$, and separated by an angular distance λ with an arm of length l. The angles (α, β) can be defined as positive or negative, allowing numerous sign combinations. See, for instance, the different hexa-rotor configurations depicted in Figure 2b; for more details, see [16]. This knowledge of the fully actuated hexa-rotor configuration is crucial for the model reference adaptive control scheme.

The existence of the tilted angles (α, β) makes possible the full actuation of the hexa-rotor at the cost of more significant power consumption. The latter is due to each motor's thrust not pointing upward as in conventional multi-rotors.

2.2 | Mathematical Model of the Hexa-Rotor

In this section, we develop the mathematical model of the fully actuated hexa-rotor depicted in Figure 1, including its rotor dynamics.

2.2.1 | Rotor Dynamics

Each rotor in the hexa-rotor system is modeled to capture the electromechanical behavior that links current input to rotor angular velocity. The equation of motion for each rotor $i \in \{1, 2, 3, 4, 5, 6\}$ is given by [49]:

$$\dot{\omega}_i = \frac{K_{T,i}}{J_{m,i}} I_i - \frac{B_{m,i}}{J_{m,i}} \omega_i, \tag{1}$$

where ω_i is the angular velocity of the i-th rotor, I_i is the input current, $K_{T,i}$ is the torque constant, and $J_{m,i}$, $B_{m,i}$ denote the rotor's inertia and viscous damping coefficient, respectively. The Coulomb friction term is assumed to be implicitly included in the damping model.

For our UAV with six motors, the motor dynamics can be compactly expressed in vector form as:

$$\dot{\omega} = -J_m^{-1} B_m \omega + J_m^{-1} K_T I, \tag{2}$$

where:

- $\omega = [\omega_1, \omega_2, \ \ldots, \omega_6]^\top \in \mathbb{R}^6$ is the vector of rotor angular velocities,
- $I = [I_1, I_2, \ \ldots, I_6]^\top \in \mathbb{R}^6$ is the vector of motor currents acting as control inputs,
- $J_m = \text{diag}(J_{m,1}, J_{m,2}, \ \ldots, J_{m,6}) \in \mathbb{R}^{6\times 6}$ is the diagonal matrix of rotor inertias,
- $K_T = \text{diag}(K_{T,1}, K_{T,2}, \ \ldots, K_{T,6}) \in \mathbb{R}^{6\times 6}$ is the diagonal matrix of motor torque constants,
- $B_m = \text{diag}(B_{m,1}, B_{m,2}, \ \ldots, B_{m,6}) \in \mathbb{R}^{6\times 6}$ is the diagonal matrix of viscous friction coefficients.

This dynamic model is used in the control allocation strategy to translate desired forces and torques into appropriate motor current commands.

With the motor model established, we now describe the 6-DOF dynamics of the fully actuated hexa-rotor.

2.2.2 | Fully Actuated Hexa-Rotor Dynamics

The hexa-rotor has 6 fixed-tilted motors indexed by $i = \{1, ..., 6\}$. Each motor is tilted with fixed angles (α_i, β_i), defining a rotation of the motor frame $\mathcal{M}_i$ w.r.t. the hexa-rotor body frame $\mathcal{B}_i$. Recall that the angular distance between motors equals λ; while the distance from each motor to the hexa-rotor center of mass is l. Thus, the mathematical model in the 6-DOF of the hexa-rotor, together with the motors' dynamics, is as follows,

$$\Sigma : \begin{cases} \dot{p} = v & \text{(3a)} \\ \dot{v} = g e_3 + \dfrac{1}{m} R u_F & \text{(3b)} \end{cases}$$

$$\Pi : \begin{cases} \dot{R} = R\hat{\Omega} & \text{(4a)} \\ \dot{\Omega} = -J^{-1}(\Omega \times J\Omega) + J^{-1} u_\tau + \Delta(t) & \text{(4b)} \end{cases}$$

$$\Gamma : \{\dot{\omega} = -J_m^{-1} B_m \omega + J_m^{-1} K_T I \tag{5a}$$

where $p = [p_x, \ p_y, \ p_z]^\top \in \mathbb{R}^3$ and $v = [v_x, \ v_y, \ v_z]^\top \in \mathbb{R}^3$ are the hexa-rotor position and velocity in the inertial frame $\mathcal{I}$ respectively; g is the gravity constant; $e_3 = [0, \ 0, \ 1]^\top \in \mathbb{R}^3$; m is the hexa-rotor mass; $R \in \text{SO}(3)$ is the rotation matrix from body to the inertial frame; $\Omega = [\omega_x, \ \omega_y, \ \omega_z]^\top \in \mathbb{R}^3$ is the angular rate; $J \in \mathbb{R}^{3\times 3}$ is the inertia matrix; the *hat* map $\hat{(\cdot)} : \mathbb{R}^3 \to \mathfrak{so}(3)$ is defined by $\hat{a}b = a \times b, \ \forall \ a, b \in \mathbb{R}^3$, and then $\hat{\Omega} \in \mathfrak{so}(3)$ is the skew-symmetric matrix of Ω; the inverse of the hat map is the *vee* map $(\cdot)^\vee : \mathfrak{so}(3) \to \mathbb{R}^3$; $u_\tau = [u_{\tau_x}, \ u_{\tau_y}, \ u_{\tau_z}]^\top \in \mathbb{R}^3$ is the torque vector considered as virtual control input for the attitude dynamics Π; $\Delta(t) = [\delta_\phi, \ \delta_\theta, \ \delta_\psi]^\top \in \mathbb{R}^3$ is an exogenous unknown disturbance due to wind gusts or similar external signals that produce undesired torques; and $u_F = [u_{F_x}, \ u_{F_y}, \ u_{F_z}]^\top \in \mathbb{R}^3$ is the

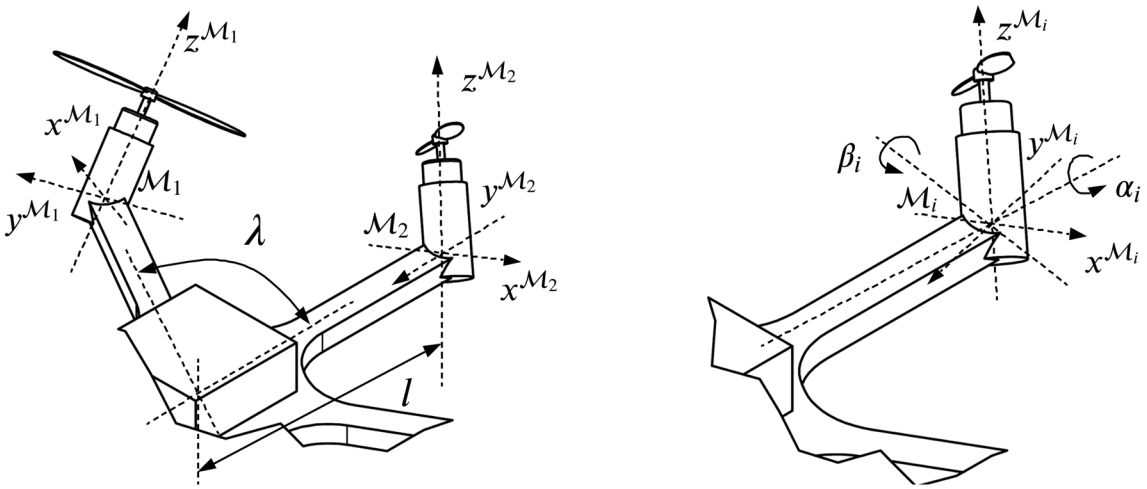

(a) Angles α_i and β_i are fixed parameters that define the tilt of each motor in its two corresponding axes.

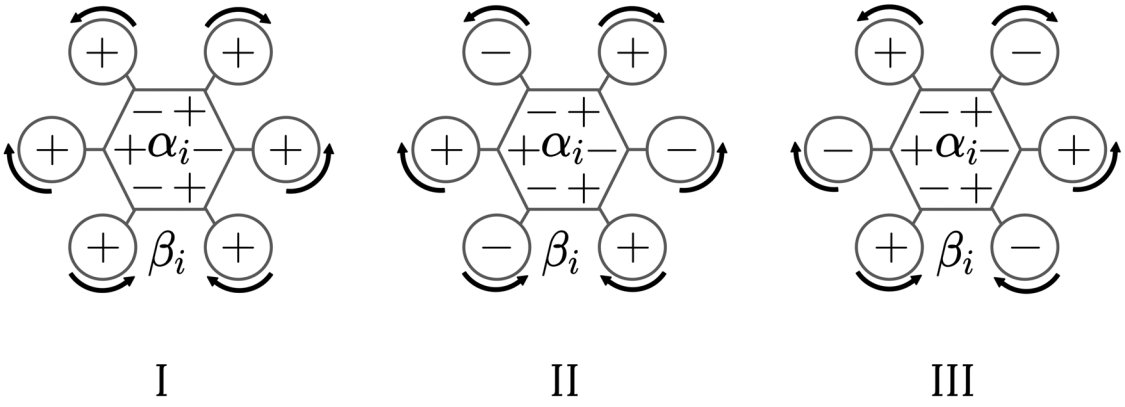

(b) Different configurations according to the arrangement of positive (+) and negative (-) values for α_i and β_i.

FIGURE 2 | A change in the sign of α_i and β_i allows having different configurations for the hexa-rotor. (a) This figure depicts how the six motors are tilted and parametrized by angles (α, β, λ) and distance l. (b) This figure shows the arrangement of the signs of α_i and β_i for the different configurations (also discussed in [16]).

force vector considered virtual control input for the position dynamics Σ. The components of the system Γ are defined identically as in Section 2.2.1.

The forces generated by the motors are modeled as,

$$u_F = \sum_{i=1}^{6} R^{\mathcal{B}}_{\mathcal{M}_i} \begin{bmatrix} 0 \\ 0 \\ -k_f \omega_i^2 \end{bmatrix} \tag{6}$$

where the term $k_f \omega_i^2$ represents the thrust generated by the i-th motor, as illustrated in Figure 1. Here, $k_f \in \mathbb{R}^+$ is the thrust coefficient, which encapsulates physical properties such as the swept rotor area, thrust generation characteristics, and dynamic pressure effects [50]. The variable ω_i denotes the rotational speed of the i-th motor. The matrix $R^{\mathcal{B}}_{\mathcal{M}_i}$ is the rotation matrix from the i-th motor frame $\mathcal{M}_i$ to the hexa-rotor's body frame $\mathcal{B}$, and is defined as:

$$R^{\mathcal{B}}_{\mathcal{M}_i}(\alpha_i,\ \beta_i,\ \lambda_i) = \begin{bmatrix} \cos\beta_i \cos\lambda_i & \cos\lambda_i \sin\alpha_i \sin\beta_i - \cos\alpha_i \sin\lambda_i & \sin\alpha_i \sin\lambda_i + \cos\alpha_i \cos\lambda_i \sin\beta_i \\ \cos\beta \sin\lambda & \cos\alpha_i \cos\lambda_1 + \sin\alpha_i \sin\beta_i \sin\lambda_i & \cos\alpha_i \sin\beta_i \sin\lambda_i - \cos\lambda_i \sin\alpha_i \\ -\sin\beta_i & \cos\beta_i \cos\alpha_i & \cos\alpha_i \sin\beta_i \end{bmatrix} \tag{7}$$

Notice that u_F in (6) can also be expressed as

$$\begin{aligned} u_F &= k_f \begin{bmatrix} R^{\mathscr{B}}_{\mathcal{M}_1}(1,3)\cdot\omega_1^2 \\ R^{\mathscr{B}}_{\mathcal{M}_1}(2,3)\cdot\omega_1^2 \\ R^{\mathscr{B}}_{\mathcal{M}_1}(3,3)\cdot\omega_1^2 \end{bmatrix} + \ldots + k_f \begin{bmatrix} R^{\mathscr{B}}_{\mathcal{M}_6}(1,3)\cdot\omega_6^2 \\ R^{\mathscr{B}}_{\mathcal{M}_6}(2,3)\cdot\omega_6^2 \\ R^{\mathscr{B}}_{\mathcal{M}_6}(3,3)\cdot\omega_6^2 \end{bmatrix} \\ &= \underbrace{k_f \begin{bmatrix} R^{\mathscr{B}}_{\mathcal{M}_1}(1,3) & R^{\mathscr{B}}_{\mathcal{M}_2}(1,3) & \cdots & R^{\mathscr{B}}_{\mathcal{M}_6}(1,3) \\ R^{\mathscr{B}}_{\mathcal{M}_1}(2,3) & R^{\mathscr{B}}_{\mathcal{M}_2}(2,3) & \cdots & R^{\mathscr{B}}_{\mathcal{M}_6}(2,3) \\ R^{\mathscr{B}}_{\mathcal{M}_1}(3,3) & R^{\mathscr{B}}_{\mathcal{M}_2}(3,3) & \cdots & R^{\mathscr{B}}_{\mathcal{M}_6}(3,3) \end{bmatrix}}_{F(\boldsymbol{\alpha},\boldsymbol{\beta},\boldsymbol{\lambda})} \underbrace{\begin{bmatrix} \omega_1^2 \\ \omega_2^2 \\ \vdots \\ \omega_6^2 \end{bmatrix}}_{\mathrm{v}} \end{aligned} \tag{8}$$

where $F \in \mathbb{R}^{3\times 6}$ and $\mathrm{v} \in \mathbb{R}^6$.

Similarly, the moments u_τ in (4b) are modeled as:

$$u_\tau = \sum_{i=1}^{6} p_i^B \times R^{\mathcal{B}}_{\mathcal{M}_i} \begin{bmatrix} 0 \\ 0 \\ -k_f \omega_i^2 \end{bmatrix} + \sum_{i=1}^{6} R^{\mathcal{B}}_{\mathcal{M}_i} \begin{bmatrix} 0 \\ 0 \\ \sigma_i d \omega_i^2 \end{bmatrix} \tag{9}$$

where p_i^B is the position of the i-th motor with respect to the body frame, and $\sigma_i \in \{-1, +1\}$ denotes the direction of rotation of rotor i (clockwise or counterclockwise). The drag torque coefficient d quantifies the reactive torque induced by aerodynamic drag on each spinning propeller. This torque is proportional to ω_i^2 and acts along the rotor's axis of rotation [50]. Besides, notice that u_τ can also be expressed as follows

$$u_\tau = \underbrace{\begin{bmatrix} C_1 & C_2 & \dots & C_6 \end{bmatrix}}_{H(\boldsymbol{\alpha},\boldsymbol{\beta},\boldsymbol{\lambda},l)} \underbrace{\begin{bmatrix} \omega_1^2 \\ \omega_2^2 \\ \vdots \\ \omega_6^2 \end{bmatrix}}_{\mathrm{v}} \tag{10}$$

where $H \in \mathbb{R}^{3\times 6}$; and $C_i \in \mathbb{R}^3$ is defined as

$$C_i = \begin{bmatrix} k_f \cdot \left(p_i^B(2) \cdot R^{\mathcal{B}}_{\mathcal{M}_i}(3,3) - p_i^B(3) \cdot R^{\mathcal{B}}_{\mathcal{M}_i}(2,3) \right) + \sigma_i d \cdot R^{\mathcal{B}}_{\mathcal{M}_i}(1,3) \\ k_f \cdot \left(p_i^B(3) \cdot R^{\mathcal{B}}_{\mathcal{M}_i}(1,3) - p_i^B(1) \cdot R^{\mathcal{B}}_{\mathcal{M}_i}(3,3) \right) + \sigma_i d \cdot R^{\mathcal{B}}_{\mathcal{M}_i}(2,3) \\ k_f \cdot \left(p_i^B(1) \cdot R^{\mathcal{B}}_{\mathcal{M}_i}(2,3) - p_i^B(2) \cdot R^{\mathcal{B}}_{\mathcal{M}_i}(1,3) \right) + \sigma_i d \cdot R^{\mathcal{B}}_{\mathcal{M}_i}(3,3) \end{bmatrix}. \tag{11}$$

Remark 1. In conventional hexa-rotors, the six matrices $R^{\mathcal{B}}_{\mathcal{M}_i}$ in (6) are the identity matrix since all the motors are perpendicular to the $x^{\mathcal{B}} - y^{\mathcal{B}}$ plane (see Figure 1). However, in the fully actuated hexa-rotor, each of the matrices $R^{\mathcal{B}}_{\mathcal{M}_i}$ is different from the identity matrix. This makes it possible for our hexa-rotor to be fully actuated.

2.3 | Problem Statement

From the motor dynamics derived in the previous subsection, it is clear that both thrust and torques generated by the fully actuated hexa-rotor are proportional to the square of the rotor angular velocities, that is, ω_i^2 for each motor $i \in \{1, \dots, 6\}$. Therefore, for control and modeling purposes, it is convenient to define the vector of squared angular velocities as:

$$\upsilon = [\omega_1^2,\ \omega_2^2,\ \dots,\ \omega_6^2]^\top. \tag{12}$$

This vector $\upsilon \in \mathbb{R}^6$ serves as the virtual control input that directly maps to the generalized force and torque vector acting on the system. As such, the total control input $u \in \mathbb{R}^6$, composed of force $u_F \in \mathbb{R}^3$ and torque $u_\tau \in \mathbb{R}^3$ components, can be compactly expressed as:

$$\underbrace{\begin{bmatrix} u_F \\ u_\tau \end{bmatrix}}_{u} = \underbrace{\begin{bmatrix} F(\alpha,\beta,\lambda) \\ H(\alpha,\beta,\lambda,l) \end{bmatrix}}_{B(\alpha,\beta,\lambda,l)} \underbrace{\begin{bmatrix} \omega_1^2 \\ \omega_2^2 \\ \vdots \\ \omega_6^2 \end{bmatrix}}_{\upsilon}, \tag{13}$$

where $B \in \mathbb{R}^{6\times 6}$, and $u, \upsilon \in \mathbb{R}^6$. If the vector υ, composed of the squared angular velocities ω_i^2 for $i = \{1, 2, \dots, 6\}$, is treated as the virtual control input for the hexa-rotor system (Σ, Π), then the system becomes fully actuated. This implies that the six degrees of freedomthree for position and three for attitudecan be controlled independently by assigning appropriate values to the six motor speeds.

Although υ is defined as a function of ω, its time evolution is not simply the square of the motor dynamics. Instead, by applying the chain rule, we obtain the derivative of υ as:

$$\dot{\upsilon} = \frac{d}{dt} \begin{bmatrix} \omega_1^2 & \omega_2^2 & \cdots & \omega_6^2 \end{bmatrix}^\top = 2\ \mathrm{diag}(\omega)\ \dot{\omega}.$$

Substituting the vectorized motor dynamics,

$$\dot{\omega} = -J_m^{-1} B_m \omega + J_m^{-1} K_T I,$$

we arrive at the evolution equation for υ:

$$\begin{aligned} \dot{\upsilon} &= 2\ \mathrm{diag}(\omega)\left(-J_m^{-1} B_m \omega + J_m^{-1} K_T I \right) \\ &= -2\ J_m^{-1} B_m \upsilon + 2\ J_m^{-1} K_T \mathrm{diag}(\omega) I. \end{aligned} \tag{14}$$

This expression provides a consistent and valid model for the squared angular velocities used in the control allocation. It links the current inputs to the system-level force and torque generation.

Let us consider (13). Since (u_F, u_τ) controls the hexa-rotor's pose, it must be considered the knowledge of the parameters (α, β, λ) for the control design. In this way, one can compute the v values in (13) that will stabilize the hexa-rotor's pose. If such parameters are precisely known, several control strategies can be applied, such as dynamic inversion or feedback linearization, as is done in [16]. Once the control algorithm is designed using any of these control techniques, one must solve the control allocation problem by solving (13). However, it is unfeasible to perform such a kind of approach if any of the parameters (α, β, λ) is not precisely known. Furthermore, the hexa-rotor's parameters can be changed according to different configurations (please see Figure 2) to obtain different desired dynamic behaviors and according to the mechanical tolerance that increases the uncertainties in the case of a small hexa-rotor. Thus, in the previous discussion, the problem of stabilization of hexa-rotor without perfect knowledge of its parameters becomes relevant.

Apart from the unknown system parameters, the hexa-rotor is considered to be affected by exogenous and unknown signals given by $\Delta(t)$, as described in the hexa-rotor mathematical model.

Considering the above, the problem statement is as follows.

Problem 1. Let's consider the nonlinear system (Σ, Π, Γ) representing the fully actuated hexa-rotor UAV, where the parameters $(\alpha, \beta, \lambda, l)$ representing the pose of the motors w.r.t. the body frame are non-precisely known. Besides, it is considered that the attitude dynamics Π are affected by exogenous and unknown disturbances. Thus, the problem is to design a control law (u_F, u_τ, r)

that globally stabilizes the origin of the dynamics of a predefined trajectory error for the above system.

Remark 2. It is worth mentioning that not every control approach is suitable for controlling every possible configuration. For instance, according to the experiments presented in [16], configuration I in Figure 2b is more challenging to control than configuration II. However, the proposed control approach can cope with all these hexa-rotor configurations.

3 | Control Strategy

This section presents the control strategy developed to obtain a feasible controller for the hexa-rotor depicted in Figure 1. For that, Problem 1 is presented as a solution.

Recalling Problem 1, there is a need for designing a robust controller to stabilize the hexa-rotor nonlinear system given by systems (Σ, Π, Γ), that is, (3), (4), and (5). The controller must consider parameter uncertainties, particularly in $(\alpha, \beta, \lambda, l)$ and the internal motor parameters (I, D). Besides, the presence of unknown disturbances in the attitude dynamics must be considered. Considering the above, a control strategy consisting of two steps is proposed:

- *Step 1*. Propose a *robust nonlinear control law* for inputs (u_F, u_τ) that globally exponentially stabilize systems (Σ, Π). The control law must be robust against exogenous disturbance in the subsystem Π.
- *Step 2*. Propose an *adaptive control law* responsible for coping with hexa-rotor parameter uncertainties $(\alpha, \beta, \lambda, l)$, including those parameters of each motor, (I, D). The adaptive control should not rely on any parameter identification or estimation strategy. In this step, the previously designed control law for (u_F, u_τ) will be used as a reference for a proposed dynamical system considering the motors' dynamics.

The control diagram of the proposed controller is depicted in Figure 3.

3.1 | Robust Nonlinear Control (Step 1)

In this step, it is intended to design a robust nonlinear control law (u_F, u_τ) that stabilizes the system (Σ, Π). Notice, however, that (u_F, u_τ) are not real control inputs, but force and torque vectors that accomplish the relation (13).[1] However, in this first step, (u_F, u_τ) are considered as virtual controls for the system (Σ, Π). Later, in step 2, control inputs will be found for the complete system with such a virtual control.

Note that Remark 1 implies that we have a full control vector $u_F = [u_{F_x},\ u_{F_y},\ u_{F_z}]^\top \in \mathbb{R}^3$, in contrast to conventional hexa-rotors where $u_F = [0,\ 0,\ f]^\top$, with f the hexa-rotor's total thrust. This point is essential for the following control strategy since it allows the independent design of the attitude and position control of the hexa-rotor system.

Assumption 1. The external disturbance $\Delta(t)$ is bounded as,

$$\|\Delta(t)\|_1 \leq c\|e_\Omega\|_1, \tag{15}$$

where $c \in \mathbb{R}_{>0}$.

The attitude control is based on the SO(3), and the aim is to stabilize both equations in subsystem Π to a desired attitude position and angular velocity given by

$$\dot{R}_d = R_d\hat{\Omega}_d, \text{ and } \hat{\Omega}_d = R_d^\top \dot{R}_d \tag{16}$$

respectively. Notice that the time derivative of the given R_d is needed to get $\hat{\Omega}_d$. In practice, this is numerically computed in the autopilot.

Theorem 1 (Attitude control). *Let us consider the attitude system* Π *in* (4) *as well as define the errors related to attitude dynamics by* [51]

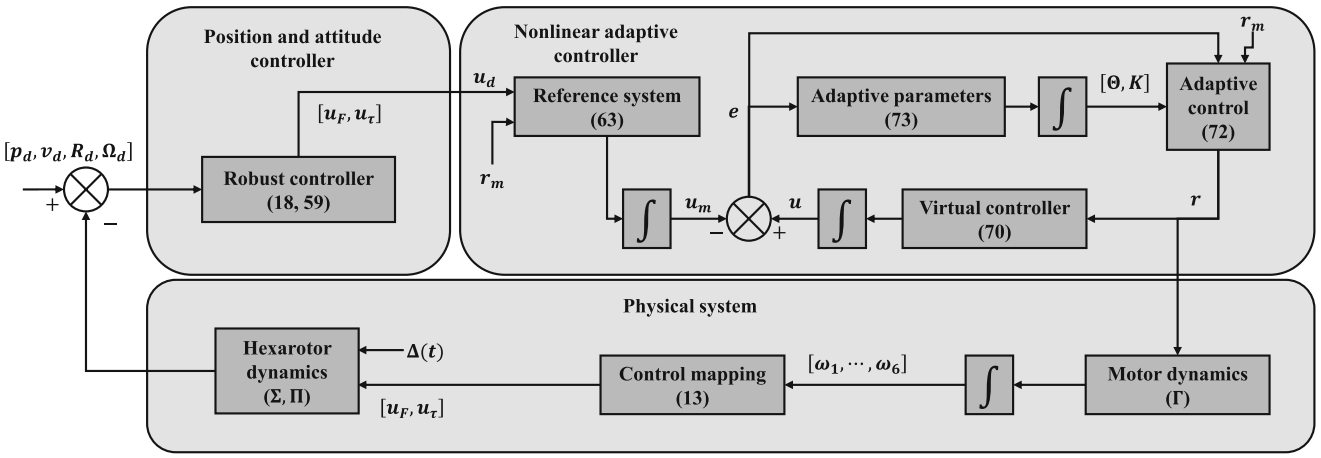

FIGURE 3 | This figure illustrates the block diagram of the proposed nonlinear robust and adaptive control system. The framework integrates a virtual and nonlinear adaptive controller to effectively handle parameter uncertainties and external disturbances. The virtual controller computes the robust control inputs, u_F, and u_τ, based on the desired states $[p_d, v_d, R_d, \Omega_d]$ and the error dynamics. These inputs are further refined by the nonlinear adaptive controller, which adapts system parameters Θ and K in real-time using a reference system and adaptation laws defined in Equations (70), (72), and (73). The outputs are applied to the physical system, including the hexa-rotor pose dynamics (Σ, Π) and motor dynamics (Γ), to achieve accurate control under uncertain and dynamic conditions.

$$
\begin{aligned}
e_R &= \frac{1}{2}\left(R_{e,r} - R_{e,r}^\top\right)^\vee = [e_R(1),\ e_R(2),\ e_R(3)]^\top,\\
e_\Omega &= \Omega - R_{e,r}^\top \Omega_d = [e_\Omega(1),\ e_\Omega(2),\ e_\Omega(3)]^\top,\\
\Psi_{SO(3)} &= \frac{1}{2} Tr(I_{3\times 3} - R_{e,r}),
\end{aligned} \tag{17}
$$

where the right attitude error is $R_{e,r} = R_d^\top R$, where R_d is the reference angular position, and $I_{3\times3}$ is the identity matrix of dimension 3. Then, the control law

$$
\begin{aligned}
u_\tau = &-J\left(k_R e_R + k_\Omega e_\Omega + k_3 \upsilon_R + k_4 \upsilon_\Omega\right) + \Omega \times J\Omega\\
&- J(\hat{\Omega} R_{e,r}^\top \Omega_d - R_{e,r}^\top \dot{\Omega}_d).
\end{aligned} \tag{18}
$$

where k_R, k_Ω, k_3, and k_4 are positive definite matrix with vector signals

$$
\upsilon_R = \begin{pmatrix} |e_R(1)|^\alpha \operatorname{sgn} e_R(1)\\ |e_R(2)|^\alpha \operatorname{sgn} e_R(2)\\ |e_R(3)|^\alpha \operatorname{sgn} e_R(3)\end{pmatrix},\ \upsilon_\Omega = \begin{pmatrix} |e_\Omega(1)|^\alpha \operatorname{sgn} e_\Omega(1)\\ |e_\Omega(2)|^\alpha \operatorname{sgn} e_\Omega(2)\\ |e_\Omega(3)|^\alpha \operatorname{sgn} e_\Omega(3)\end{pmatrix} \tag{19}
$$

with a positive real number $\alpha < 1$ exponentially stabilizes the zero-equilibrium points (17).

Proof. Let us begin by computing the error dynamics of Equation (17) as follows,

$$
\begin{aligned}
\Psi_{SO(3)} &= \frac{1}{2} e_\Omega^\top \left(R_d^\top R - R^\top R_d\right)^\vee = e_R^\top e_\Omega\\
\dot{e}_R &= \frac{1}{2}\left(R_d^\top R \hat{e}_\Omega + \hat{e}_\Omega R^\top R_d\right)\\
&= \underbrace{\frac{1}{2}\left(Tr\left[R^\top R_d\right] I_3 - R^\top R_d\right)}_{C(R_d,R)} e_\Omega\\
\dot{e}_\Omega &= J^{-1}\tau - J^{-1}\Omega \times J\Omega + \left(\hat{\Omega} R^\top R_d \Omega_d - R^\top R_d \dot{\Omega}_d\right)\\
&\quad + \Delta_\Omega(t).
\end{aligned} \tag{20}
$$

The last equation with the proposed control (18) results in:

$$
\dot{e}_\Omega = -\left(K_R e_R + K_\Omega e_\Omega + K_3 \upsilon_R + K_4 \upsilon_\Omega\right) + \Delta_\Omega(t). \tag{21}
$$

Let the candidate Lyapunov function

$$
\begin{aligned}
V(R, R_d, \Omega, \Omega_d) = &\underbrace{e_R^\top e_\Omega}_{V_1} + \underbrace{\frac{1}{2} e_\Omega^\top J A e_\Omega}_{V_2}\\
&+ \underbrace{\frac{d}{2} Tr(I_3 - R_d^\top R)}_{V_3} + \underbrace{\operatorname{sgn} e_\Omega^\top B e_\Omega}_{V_4},
\end{aligned} \tag{22}
$$

where $A \in \mathbb{R}^{3\times3}$ is a positive definite matrix, $B \in \mathbb{R}^{3\times3}$ is a diagonal and positive definite matrix, and

$$
\operatorname{sgn} e_R = \begin{pmatrix} \operatorname{sgn} e_R(1)\\ \operatorname{sgn} e_R(2)\\ \operatorname{sgn} e_R(3)\end{pmatrix},\ \operatorname{sgn} e_\Omega = \begin{pmatrix} \operatorname{sgn} e_\Omega(1)\\ \operatorname{sgn} e_\Omega(2)\\ \operatorname{sgn} e_\Omega(3)\end{pmatrix}. \tag{23}
$$

Now, let us compute the time derivative of V. For easy interpretation, let begin by computing $\dot{V}_1$ as follows

$$
\begin{aligned}
\dot{V}_1 = \dot{e}_R^\top e_\Omega + e_R^\top \dot{e}_\Omega = e_\Omega^\top C(R_d, R)^\top e_\Omega + e_R^\top\big(&J^{-1}\tau - J^{-1}\Omega\\
&\times J\Omega + \left(\hat{\Omega} R^\top R_d \Omega_d - R^\top R_d \dot{\Omega}_d\right) + \Delta_\Omega(t)\big)
\end{aligned} \tag{24}
$$

then, substitute (18) in the previous equation,

$$
\begin{aligned}
\dot{V}_1 = e_\Omega^\top C(R_d, R)^\top e_\Omega + e_R^\top\big(&-K_R e_R - K_\Omega e_\Omega\\
&- K_3 \upsilon_R - K_4 \upsilon_\Omega + \Delta_\Omega(t)\big)
\end{aligned} \tag{25}
$$

and since $\|C(R_d, R)\|_2 \le 1$, it follows that

$$
\begin{aligned}
\dot{V}_1 \le \|e_\Omega\|_2^2 - e_R^\top K_R e_R - e_R^\top K_\Omega e_\Omega - |e_R|^\top K_3 |e_R|^\alpha\\
+ \|K_4\| |e_R|^\top |e_\Omega|^\alpha + e_R^\top \Delta_\Omega(t)
\end{aligned} \tag{26}
$$

where

$$
\begin{aligned}
|e_R| &= \begin{pmatrix} |e_R(1)|\\ |e_R(2)|\\ |e_R(3)|\end{pmatrix},\quad |e_R|^\alpha = \begin{pmatrix} |e_R(1)|^\alpha\\ |e_R(2)|^\alpha\\ |e_R(3)|^\alpha\end{pmatrix},\\
|e_\Omega| &= \begin{pmatrix} |e_\Omega(1)|\\ |e_\Omega(2)|\\ |e_\Omega(3)|\end{pmatrix},\quad |e_\Omega|^\alpha = \begin{pmatrix} |e_\Omega(1)|^\alpha\\ |e_\Omega(2)|^\alpha\\ |e_\Omega(3)|^\alpha\end{pmatrix}.
\end{aligned} \tag{27}
$$

Now, let us continue by computing the time derivative of V_2 in (22) along the trajectories of (21) as follows,

$$
\begin{aligned}
\dot{V}_2 &= e_\Omega^\top J A \dot{e}_\Omega = e_\Omega^\top J A\big(-K_R e_R - K_\Omega e_\Omega - K_3 \upsilon_R\\
&\quad - K_4 \upsilon_\Omega + \Delta_\Omega(t)\big)\\
&= -e_\Omega^\top (J A K_R) e_R - e_\Omega^\top (J A K_\Omega) e_\Omega - e_\Omega^\top (J A K_3) \upsilon_R\\
&\quad - e_\Omega^\top (J A K_4) \upsilon_\Omega + e_\Omega^\top (J A) \Delta_\Omega(t)\\
&\le -e_R^\top (J A K_R) e_\Omega - e_\Omega^\top (J A K_\Omega) e_\Omega + |e_\Omega|^\top J A K_3 |e_R|^\alpha\\
&\quad - |e_\Omega|^\top J A K_4 |e_\Omega|^\alpha + e_\Omega^\top (J A) \Delta_\Omega(t).
\end{aligned} \tag{28}
$$

Let us compute $\dot{V}_3$ as,

$$
\dot{V}_3 = \frac{d}{2}\frac{d}{dt} Tr(I_3 - R_d^\top R) = -\frac{d}{2} Tr\left(\frac{d}{dt}\left(R_d^\top R\right)\right) \tag{29}
$$

and since

$$
\begin{aligned}
\frac{d}{dt}\left(R_d^\top R\right) &= \frac{d}{dt}(R_d^\top) R + R_d^\top \frac{d}{dt}(R) = \hat{\Omega}_d^\top R_d^\top R + R_d^\top R \hat{\Omega}\\
&= R_d^\top R \left(\underbrace{R^\top R_d \hat{\Omega}_d^\top R_d^\top R}_{-(R^\top R_d \Omega_d)^\wedge} + \hat{\Omega}\right),
\end{aligned} \tag{30}
$$

where (4) and (16) are used together with the property $R\hat{a}R^\top = (Ra)^\wedge$ where $a \in \mathbb{R}^3$ and $R \in SO(3)$, and the fact that $\hat{\Omega}_d^\top = -\hat{\Omega}_d$. Then, it follows that,

$$
\frac{d}{dt}\left(R_d^\top R\right) = R_d^\top R \hat{e}_\Omega. \tag{31}
$$

Finally, from the last expression, it is clear that,

$$\begin{aligned}\dot{V}_3 &= -\frac{d}{2}Tr\left(R_d^\top R\hat{e}_\Omega\right) = \frac{d}{2}e_\Omega^\top(R_d^\top R - R^\top R_d)\\ &= e_\Omega^\top D e_R = e_R^\top D e_\Omega,\end{aligned} \tag{32}$$

where the property $Tr(A\hat{a}) = -a^\top(A - A^\top)^\vee$ is used. From here, a is defined as above, and $A \in \mathbb{R}^{3\times3}$. The diagonal matrix D is chosen accordingly.

Finally, the time derivative of V_4 is computed as follows,

$$\begin{aligned}\dot{V}_4 &= \operatorname{sgn} e_\Omega^\top B\left(-K_R e_R - K_\Omega e_\Omega - K_3 \upsilon_R - K_4 \upsilon_\Omega + \Delta_\Omega(t)\right)\\ &\leq \operatorname{sgn} e_R^\top(BK_R)e_R - \operatorname{sgn} e_\Omega^\top(BK_\Omega)e_\Omega + (|e_R|^{\frac{\alpha}{2}})^\top(BK_3)|e_R|^{\frac{\alpha}{2}}\\ &\quad - (|e_\Omega|^{\frac{\alpha}{2}})^\top(BK_4)|e_\Omega|^{\frac{\alpha}{2}} + \|B\Delta_\Omega(t)\|.\end{aligned} \tag{33}$$

Then, the following must be computed,

$$\begin{aligned}\dot{V} \leq\ & \|e_\Omega\|_2^2 - e_R^\top K_R e_R - e_R^\top K_\Omega e_\Omega - |e_R|^\top K_3|e_R|^\alpha\\ &+ \|K_4\||e_R|^\top|e_\Omega|^\alpha + e_R^\top\Delta_\Omega(t)\\ &- e_R^\top(JAK_R)e_\Omega - e_\Omega^\top(JAK_\Omega)e_\Omega + |e_\Omega|^\top JAK_3|e_R|^\alpha\\ &- |e_\Omega|^\top JAK_4|e_\Omega|^\alpha + e_\Omega^\top(JA)\Delta_\Omega(t)\\ &+ e_R^\top D e_\Omega + \operatorname{sgn} e_R^\top(BK_R)e_R - \operatorname{sgn} e_\Omega^\top(BK_\Omega)e_\Omega\\ &+ (|e_R|^{\frac{\alpha}{2}})^\top(BK_3)|e_R|^{\frac{\alpha}{2}} - (|e_\Omega|^{\frac{\alpha}{2}})^\top(BK_4)|e_\Omega|^{\frac{\alpha}{2}} + \|B\Delta_\Omega(t)\|.\end{aligned} \tag{34}$$

Grouping all the terms, it follows that,

$$\begin{aligned}\dot{V} \leq\ & -e_R^\top K_R e_R - |e_R|^\top K_3|e_R|^\alpha + \operatorname{sgn} e_R^\top(BK_R)e_R\\ &+ (|e_R|^{\frac{\alpha}{2}})^\top(BK_3)|e_R|^{\frac{\alpha}{2}}\end{aligned} \tag{35}$$

$$\begin{aligned}&- e_\Omega^\top(JAK_\Omega)e_\Omega - |e_\Omega|^\top JAK_4|e_\Omega|^\alpha - \operatorname{sgn} e_\Omega^\top(BK_\Omega)e_\Omega\\ &- (|e_\Omega|^{\frac{\alpha}{2}})^\top(BK_4)|e_\Omega|^{\frac{\alpha}{2}} + \|e_\Omega\|_2^2\end{aligned} \tag{36}$$

$$- e_R^\top K_\Omega e_\Omega - e_R^\top(JAK_R)e_\Omega + e_R^\top D e_\Omega \tag{37}$$

$$+ e_R^\top\Delta_\Omega(t) + e_\Omega^\top(JA)\Delta_\Omega(t) + \|B\Delta_\Omega(t)\| \tag{38}$$

$$+ \|K_4\||e_R|^\top|e_\Omega|^\alpha + |e_\Omega|^\top JAK_3|e_R|^\alpha. \tag{39}$$

Let's begin with the positive terms of (35) by noting that

$$\begin{aligned}&\operatorname{sgn} e_R^\top(BK_R)e_R + (|e_R|^{\frac{\alpha}{2}})^\top(BK_3)|e_R|^{\frac{\alpha}{2}}\\ &= (|e_R|^\alpha)^\top(BK_R)|e_R|^\beta + (|e_R|^{\frac{\alpha}{2}})^\top(BK_3)|e_R|^{\frac{\alpha}{2}}\\ &\leq 2^\beta(|e_R|^{\frac{\alpha}{2}})^\top(BK_R)|e_R|^{\frac{\alpha}{2}} + (|e_R|^{\frac{\alpha}{2}})^\top(BK_3)|e_R|^{\frac{\alpha}{2}}\\ &\leq (|e_R|^{\frac{\alpha}{2}})^\top(B[2^\beta K_R + K_3])|e_R|^{\frac{\alpha}{2}}\end{aligned} \tag{40}$$

where it is assumed that $\alpha + \beta = 1$, and the fact that $\||e_R|\| \leq 2$. And then, (35) is simplified to

$$-e_R^\top K_R e_R - |e_R|^\top K_3|e_R|^\alpha + (|e_R|^{\frac{\alpha}{2}})^\top(B[2^\beta K_R + K_3])|e_R|^{\frac{\alpha}{2}} \tag{41}$$

Now, for (36):

$$\begin{aligned}&-e_\Omega^\top(JAK_\Omega - I_{3\times3})e_\Omega - |e_\Omega|^\top JAK_4|e_\Omega|^\alpha\\ &- \operatorname{sgn} e_\Omega^\top(BK_\Omega)e_\Omega - (|e_\Omega|^{\frac{\alpha}{2}})^\top(BK_4)|e_\Omega|^{\frac{\alpha}{2}}\end{aligned} \tag{42}$$

Next, (37) can simplified as:

$$-e_R^\top K_\Omega e_\Omega - e_R^\top(JAK_R)e_\Omega + e_R^\top D e_\Omega = 0 \tag{43}$$

as long as $D = K_\Omega + JAK_R$ is defined.

Then, (38) is simplified by taking into account assumption 1 as follows,

$$\begin{aligned}e_R^\top\Delta_\Omega(t) + e_\Omega^\top(JA)\Delta_\Omega(t) + \|B\Delta_\Omega(t)\| &\leq c\|e_R^\top\|\|e_\Omega\|\\ &+ \underbrace{e_\Omega^\top(cJA)e_\Omega}_{\text{1-norm}} + \underbrace{(\operatorname{sgn} e_\Omega)^\top cBe_\Omega}_{\text{1-norm}}\end{aligned} \tag{44}$$

Finally, (39) is simplified by using the Young inequality, and considering that $\alpha = 1/2$:

$$\begin{aligned}&|e_R|^\top K_4|e_\Omega|^\alpha + |e_\Omega|^\top JAK_3|e_R|^\alpha\\ &\leq \|(|e_\Omega|^\alpha)^\top\|_1\|K_4\|_1\||e_R|\|_2 + \||e_\Omega|^\top\|_1\|JAK_3\|_1\||e_R|^\alpha\|_2\\ &\leq \frac{\|K_4\|^2|e_R|^\top|e_R|}{2} + \frac{(|e_\Omega|^{\frac{1}{2}})^\top|e_\Omega|^{\frac{1}{2}}}{2} + (|e_\Omega|^{\frac{1}{2}})^\top\\ &(2^\alpha\|JAK_3\|_1 I_{3\times3})|e_\Omega|^{\frac{1}{2}}.\end{aligned} \tag{45}$$

Put together with all the simplifications, the following expression is obtained:

$$\begin{aligned}\dot{V} \leq\ & -e_R^\top K_R e_R - |e_R|^\top K_3|e_R|^\alpha + (|e_R|^{\frac{\alpha}{2}})^\top(B[2^\beta K_R + K_3])|e_R|^{\frac{\alpha}{2}}\\ &- e_\Omega^\top(JAK_\Omega - I_{3\times3})e_\Omega - |e_\Omega|^\top JAK_4|e_\Omega|^\alpha\\ &- \operatorname{sgn} e_\Omega^\top(BK_\Omega)e_\Omega - (|e_\Omega|^{\frac{\alpha}{2}})^\top(BK_4)|e_\Omega|^{\frac{\alpha}{2}}\\ &+ c\|e_R^\top\|\|e_\Omega\| + e_\Omega^\top(cJA)e_\Omega + (\operatorname{sgn} e_\Omega)^\top cBe_\Omega\\ &+ \left(|e_\Omega|^{\frac{\alpha}{2}}\right)^\top(2\|K_4\|_1 I_{3\times3})\left(|e_\Omega|^{\frac{\alpha}{2}}\right)\\ &+ (\operatorname{sgn} e_\Omega)^\top(2^\alpha\|JAK_3\|_1 I_{3\times3})e_\Omega,\end{aligned} \tag{46}$$

which can be rearranged as,

$$\begin{aligned}\dot{V} \leq\ & -e_R^\top K_R e_R - (|e_R|^{\frac{1}{2}(\alpha+1)})^\top K_3|e_R|^{\frac{1}{2}(\alpha+1)}\\ &+ (|e_R|^{\frac{\alpha}{2}})^\top(B[2^\beta K_R + K_3])|e_R|^{\frac{\alpha}{2}}\\ &- e_\Omega^\top(JAK_\Omega - I_{3\times3} - cJA)e_\Omega - (|e_\Omega|^{\frac{1}{2}(\alpha+1)})^\top JAK_4|e_\Omega|^{\frac{1}{2}(\alpha+1)}\\ &- (|e_\Omega|^{1/2})^\top(BK_\Omega - cB - 2^\alpha\|JAK_3\|_1 I_{3\times3})|e_\Omega|^{1/2}\\ &- (|e_\Omega|^{\frac{\alpha}{2}})^\top(BK_4 - 2\|K_4\|_1 I_{3\times3})|e_\Omega|^{\frac{\alpha}{2}}\\ &+ c\|e_R^\top\|\|e_\Omega\|.\end{aligned} \tag{47}$$

The last two terms in the first row of the previous equation can be arranged as:

$$\begin{aligned}&-(|e_R|^{\frac{1}{2}(\alpha+1)})^\top K_3|e_R|^{\frac{1}{2}(\alpha+1)} + (|e_R|^{\frac{\alpha}{2}})^\top(B[2^\beta K_R + K_3])|e_R|^{\frac{\alpha}{2}}\\ &= -(|e_R|^{\frac{1}{2}(\alpha+1)})^\top\times\\ &\left[K_3 - I_{3\times3}\odot|e_R|^{-1}1^\top B(2^\beta K_R + K_3)\right]|e_R|^{\frac{1}{2}(\alpha+1)}\end{aligned} \tag{48}$$

where

$$|e_R|^{-1} = \begin{pmatrix} |e_R(1)|^{-1} \\ |e_R(2)|^{-1} \\ |e_R(3)|^{-1} \end{pmatrix} \tag{49}$$

and $\odot$ is the Hadamard product, and $1^\top = [1,\ 1,\ 1]$. Notice that the RHS of (48) must be positive, and hence

$$\begin{aligned} K_3 &> I_{3\times3} \odot |e_R|^{-1} 1^\top B(2^\beta K_R + K_3) \\ (K_3)(2^\beta K_R + K_3)^{-1}(B)^{-1} &> I_{3\times3} \odot |e_R|^{-1} 1^\top \\ I_{3\times3} \odot |e_R| 1^\top &> (B)(2^\beta K_R + K_3)(K_3)^{-1}, \end{aligned} \tag{50}$$

which, after simple computations, it follows that:

$$|e_R(i)| > b_i \frac{2^\beta k_{R_i} + k_{3_i}}{k_{3_i}}, \tag{51}$$

for $i = \{1, 2, 3\}$. From (51) one can choose k_{3_i} arbitrarily large, and b_i arbitrarily small so that the right-hand side of (51) is arbitrarily close to zero.

Thus,

$$\dot{V} \leq -\zeta^\top Z \zeta, \tag{52}$$

where

$$\zeta = \left(|e_R|,\ |e_R|^{\frac{1}{2}(\alpha+1)},\ |e_\Omega|,\ |e_\Omega|^{\frac{1}{2}(\alpha+1)},\ |e_\Omega|^{\frac{\alpha}{2}},\ |e_\Omega|^{\frac{1}{2}} \right)^\top, \tag{53}$$

and

$$Z = \begin{pmatrix} K_R - \frac{\|K_4\|^2}{2} & 0 & -\frac{c}{2} & 0 & 0 & 0 \\ 0 & K_3 - \epsilon I_{3\times3} & 0 & 0 & 0 & 0 \\ -\frac{c}{2} & 0 & JAK_\Omega - I_{3\times3} - cJA & 0 & 0 & 0 \\ 0 & 0 & 0 & JAK_4 & 0 & 0 \\ 0 & 0 & 0 & 0 & BK_4 & 0 \\ 0 & 0 & 0 & 0 & 0 & BK_\Omega - cB - (2^\alpha \|JAK_3\|_1 - \frac{1}{2}) I_{3\times3} \end{pmatrix}, \tag{54}$$

where ϵ is a small positive number coming from (51). Besides,

$$\begin{aligned} BK_\Omega - cB - \left(2^\alpha \|JAK_3\|_1 - \frac{1}{2}\right) I_{3\times3} &> 0_{3\times3} \\ B(K_\Omega - cI_{3\times3}) &> \left(2^\alpha \|JAK_3\|_1 - \frac{1}{2}\right) I_{3\times3} \\ K_\Omega &> B^{-1}\left(2^\alpha \|JAK_3\|_1 \right. \\ &\quad \left. -\frac{1}{2} + cB\right) I_{3\times3} \end{aligned} \tag{55}$$

and the following inequalities must hold,

$$\begin{aligned} K_R &> \frac{\|K_4\|^2}{2} \\ K_3 &> \epsilon I_{3\times3} \\ K_\Omega &> A^{-1}J^{-1}(cJA + I_{3\times3}). \end{aligned} \tag{56}$$

Achieving that all the above inequalities hold is possible, and thus, all the eigenvalues of the above matrix are clearly positive. This implies that such a matrix is positively definite and that stability is achieved. □

Remark 3. Notice that the control terms in (19) are not differentiable at zero. Since we later require the time derivative of the position control vector u in (13), a smooth approximation is implemented for numerical robustness. Specifically, instead of using the non-smooth terms υ_R and υ_Ω defined in (19), we implement their smoothed versions as:

$$\begin{aligned} \upsilon_R &= \begin{pmatrix} \left(e_R(1)^2 + \delta\right)^{\frac{\alpha}{2}} \tanh(\gamma e_R(1)) \\ \left(e_R(2)^2 + \delta\right)^{\frac{\alpha}{2}} \tanh(\gamma e_R(2)) \\ \left(e_R(3)^2 + \delta\right)^{\frac{\alpha}{2}} \tanh(\gamma e_R(3)) \end{pmatrix}, \\ \upsilon_\Omega &= \begin{pmatrix} \left(e_\Omega(1)^2 + \delta\right)^{\frac{\alpha}{2}} \tanh(\gamma e_\Omega(1)) \\ \left(e_\Omega(2)^2 + \delta\right)^{\frac{\alpha}{2}} \tanh(\gamma e_\Omega(2)) \\ \left(e_\Omega(3)^2 + \delta\right)^{\frac{\alpha}{2}} \tanh(\gamma e_\Omega(3)) \end{pmatrix}, \end{aligned} \tag{57}$$

where $\delta > 0$ is a small smoothing constant, γ is a positive gain, and $\alpha \in (0, 1)$ determines the level of nonlinearity. This modification preserves the finite-time convergence properties while ensuring differentiability around the origin.

The position control is given in the following theorem.

Theorem 2 (Position control). *Let us consider the position system Σ in* (3)*, and define the position and velocity errors as follows,*

$$e_p = p - p_d, \quad \dot{e}_p = \dot{p} - \dot{p}_d \tag{58}$$

where $e_p = [e_{p_x},\ e_{p_y},\ e_{p_z}]^\top$; and $p_d \in \mathbb{R}^3$ is a smooth desired position trajectory. Then, the control law

$$u_F = -mR^\top \left(ge_3 + k_1 e_p + k_2 \dot{e}_p - \ddot{p}_d\right), \tag{59}$$

where (k_1, k_2) are positive numbers, globally asymptotically stabilizes the zero-equilibrium points (58).

Proof. Let us consider the errors (58), so that the following candidate Lyapunov function is proposed:

$$V_1(e_p, \dot{e}_p) = \frac{1}{2} k_1 e_p^\top e_p + \frac{1}{2} \dot{e}_p^\top \dot{e}_p \tag{60}$$

with time derivative

$$\dot{V}_1(e_p, \dot{e}_p) = k_1 e_p^\top \dot{e}_p + \dot{e}_p^\top \ddot{e}_p. \tag{61}$$

Since $\ddot{e}_p = \dot{v} - \ddot{p}_d$, (3b) and the control (59) are substituted in the last expression to get:

$$\begin{aligned}\dot{V}_1(e_p, \dot{e}_p) &= k_1 e_p^\top \dot{e}_p + \dot{e}_p^\top (g e_3 + \frac{1}{m} R u_F - \ddot{p}_d) \\ &= k_1 e_p^\top \dot{e}_p + \dot{e}_p^\top (-k_1 e_p - k_2 \dot{e}_p) \\ &= -k_2 \dot{e}_p^\top \dot{e}_p \leq 0. \end{aligned} \tag{62}$$

To prove that the closed-loop system Σ with the control (59) is asymptotically stable, the LaSalle invariance principle is claimed, in which needs to be proven that the set $\Xi = \{(e_p, \dot{e}_p) \mid \dot{V}_1(e_p, \dot{e}_p) = 0\}$ contains only the equilibrium point $[e_p,\ \dot{e}_p]^\top = [0,\ 0]^\top$. First, notice that the expression $\dot{V}_1(e_p, \dot{e}_p) = 0$ in the set Ξ together with (62) means that $\dot{e}_p = 0$. Also, from the closed-system error dynamics $\ddot{e}_p = -k_1 e_p - k_2 \dot{e}_p = 0$, it follows that $e_p = 0$. Hence, the only solution that is contained in Ξ is the equilibrium point $[e_p,\ \dot{e}_p] = [0,\ 0]^\top$. Thus, since V_1 is radially unbounded, the zero-equilibrium point (58) is globally asymptotically stable, and the proof is completed. □

Once the virtual controls (u_F, u_τ) have been designed, one needs to solve Equation (13) for the motor's angular velocities v. This is called *control allocation problem*, and can be easily solved once we exactly know the values of parameters $(\boldsymbol{\alpha}, \boldsymbol{\beta}, \boldsymbol{\lambda})$. However, from Problem 1, such parameters can vary and are considered unknown. Thus, the second step in the proposed control approach is to design an adaptive control based on a reference model that copes with such a restriction. This requirement is detailed next.

3.2 | Adaptive Control (Step 2)

A *model reference adaptive control* approach is developed for the second step of the proposed approach. The reference model is responsible for providing a tool to help the fully actuated hexa-rotor to track the virtual controls (u_τ, u_F) in (18) and (59) despite the lack of knowledge of the system parameters. The reference model is designed as

$$\dot{u}_m = A_m u_m + G_m r_m, \tag{63}$$

where $A_m \in \mathbb{R}^{6\times6}$ is a Hurwitz matrix; $G_m \in \mathbb{R}^{6\times6}$ is an invertible matrix; and $r_m \in \mathbb{R}^6$ is the control input. Here, the goal is to design r_m such that $u_m \in \mathbb{R}^6$ reach the desired trajectory $u_d = [u_F,\ u_\tau]^\top \in \mathbb{R}^6$, given by the previous designed controls (18) and (59).

The following assumption is required for the adaptive control scheme proposed in this design step.

Assumption 2. The control (u_F, u_τ) is first-time differentiable.

One of the main results of this design step is presented next.

Lemma 1. *Let us consider that Assumption 2 holds. Then, the control law*

$$r_m = -G_m^{-1} \tilde{K} \tilde{u} - G_m^{-1} A_m u_m + G_m^{-1} \dot{u}_d, \tag{64}$$

where $\tilde{K} \in \mathbb{R}^{6\times6}$ is a stable matrix, globally exponentially stabilizes the origin

$$\tilde{u} = u_m - u_d = 0_{6\times1} \in \mathbb{R}^6 \tag{65}$$

of the error system,

$$\dot{\tilde{u}} = A_m u_m + G_m r_m - \dot{u}_d. \tag{66}$$

Proof. Let us consider the candidate Lyapunov function $V_{\tilde{u}} = \tilde{u}^\top P_{\tilde{u}} \tilde{u}$ where $P_{\tilde{u}}$ is a symmetric positive definite matrix such that $\tilde{K}^\top P + P\tilde{K} = -Q_{\tilde{u}} < 0$ holds, for a positive definite matrix $Q_{\tilde{u}}$. The time derivative of $V_{\tilde{u}}$ along the trajectories of the system (66), together with control (64) is computed as follows:

$$\begin{aligned}\dot{V}_{\tilde{u}} &= \dot{\tilde{u}}^\top P_{\tilde{u}} \tilde{u} + \tilde{u}^\top P_{\tilde{u}} \dot{\tilde{u}} \\ &= \left(u_m^\top A_m^\top + r_m^\top G_m^\top - \dot{u}_d^\top\right) P_{\tilde{u}} \tilde{u} + \tilde{u}^\top P_{\tilde{u}} \left(A_m u_m + G_m r_m - \dot{u}_d\right), \end{aligned} \tag{67}$$

and after substituting the control (64) into the previous expression, it follows that,

$$\dot{V}_{\tilde{u}} = \tilde{u}^\top \left(\tilde{K}^\top P_{\tilde{u}} + P_{\tilde{u}} \tilde{K}\right) \tilde{u} = -\tilde{u}^\top Q \tilde{u} \tag{68}$$

and thus, u_m follows u_d globally exponentially, and the proof is complete. □

Now, please recall Equation (13), where the square matrix $B(\alpha, \beta, \lambda, l) \in \mathbb{R}^{6\times6}$ represents the static control allocation map and satisfies the following assumption:

Assumption 3. To ensure the hexa-rotor's controllability, the matrix,

$$B = \begin{bmatrix} F(\alpha, \beta, \lambda) \\ H(\alpha, \beta, \lambda, l) \end{bmatrix}$$

is invertible.[2]

Moreover, note that $\upsilon := [\omega_1^2, \omega_2^2, \ldots, \omega_6^2]^\top \in \mathbb{R}^6$ corresponds to the squared angular velocities of the motors, which act as virtual control signals for stabilizing the fully actuated hexa-rotor pose. Thus, recalling that $u = B\upsilon$ from (13), we define a virtual dynamical system governed by:

$$\dot{u} = B\dot{\upsilon}, \tag{69}$$

which describes the rate of change of the total forces and torques generated by the spinning motors. Finally, combining Equations (69) and (14), the full expression for the virtual control derivative becomes:

$$\dot{u} = \underbrace{-2B\ J_m^{-1} B_m B^{-1}}_{A} u + \underbrace{2B\ J_m^{-1} K_T}_{G} \underbrace{\operatorname{diag}(\omega) I}_{r}, \tag{70}$$

where $A = B\ J_m^{-1} B_m B^{-1}$ and $G = 2B\ J_m^{-1} K_T$ are matrices containing all the unknown system parameters, including those of the motors' system Γ; the variable $r = \operatorname{diag}(\omega) I$ is considered the control input. Equation (70) links the evolution of the generated forces and torques to the internal motor dynamics.

Besides, the matrix G above is assumed to fulfill the following assumption.

Assumption 4. Matrix G in (70) can be decomposed using the matrix sign decomposition [52], where S (the sign matrix) gathers only the information about the type of configuration,

$$G = SN, \;\; S = \text{sgn}\,(G), \;\; G \in \mathbb{R}^{n\times n}. \tag{71}$$

Also, if $G = Z\text{diag}(J(\lambda_k))Z^{-1}$ is a Jordan decomposition, then

$$S = Z\text{diag}(\text{sgn}\,(\lambda_k))Z^{-1}, \text{ and } N = Z\text{diag}(\text{sgn}\,(\lambda_k))\,\text{diag}\,(J(\lambda_k))Z^{-1},$$

where λ_k are the eigenvalues of G. In accordance with the matrix sign function theory [52], we assume that G has no purely imaginary eigenvalues. For complex eigenvalues, the sign is taken with respect to the real part, that is, $\text{sgn}\,(\lambda_k) := \text{sgn}\,(\Re(\lambda_k))$, so that S remains real and well-defined. Notice that S, N and G commute with each other.

Next, the second element in the main results is presented: the adaptive control that will ensure that $u \in \mathbb{R}^6$ in (70) will converge to $u_d = [u_F, \; u_\tau]^\top$.

Theorem 3. *Let us consider the dynamical system (70) together with the reference model (63). Also, consider that Assumption 4 holds for G in (70). Let the adaptive control law be given by*

$$r = \Theta u + K r_m, \tag{72}$$

where r_m is defined as in (64), and $\Theta, K \in \mathbb{R}^{6\times 6}$ are adaptive parameters governed by the update laws:

$$\begin{aligned} \dot{\Theta}^\top &= -ue^\top PS, \\ \dot{K}^\top &= -r_m e^\top PS, \end{aligned} \tag{73}$$

where $P \in \mathbb{R}^{6\times 6}$ is a positive definite matrix such that $PA_m + A_m^\top P = -Q$, with Q symmetric positive definite, and $S \in \mathbb{R}^{6\times 6}$ is the sign matrix of G. Define the tracking error and parameter errors as:

$$e = u - u_m, \quad \Phi = \Theta - \Theta^*, \quad \Psi = K - K^*, \tag{74}$$

where the ideal parameter values Θ^* and K^* are given by:

$$\Theta^* = G^{-1}(A_m - A), \quad K^* = G^{-1}G_m. \tag{75}$$

Then, the tracking error globally asymptotically converges to zero, that is, $e(t) \to 0$ as $t \to \infty$ for all initial conditions. Moreover, the parameter error derivatives satisfy $\dot{\Phi}(t) \to 0$ and $\dot{\Psi}(t) \to 0$ as $t \to \infty$.

Proof. The error dynamics of the first equation in (74) is given by,

$$\begin{aligned} \dot{e} = \dot{u} - \dot{u}_m &= Au + Gr - A_m u_m - G_m r_m \\ &= Au + G\big(\Theta u + K r_m\big) - A_m u_m - G_m r_m \\ &= Au + G\big(\Phi + \Theta^*\big)u + G(\Psi + K^*)r_m - A_m u_m - G_m r_m, \end{aligned} \tag{76}$$

and after substituting (75) into the previous expression it follows that,

$$\begin{aligned} \dot{e} &= Au + G\Phi u + \big(A_m - A\big)u + G\Psi r_m + G_m r_m - A_m u_m - G_m r_m \\ &= G\Phi u + A_m u + G\Psi r_m - A_m u_m \\ &= A_m e + G\Phi u + G\Psi r_m. \end{aligned} \tag{77}$$

Now, let us propose the candidate Lyapunov function,

$$V_2(e, \Phi, \Psi) = e^\top Pe + Tr\big[\Phi^\top N\Phi\big] + Tr\big[\Psi^\top N\Psi\big], \tag{78}$$

with time derivative along the trajectories of the error system (76) given by

$$\begin{aligned} \dot{V}_2(e, \Phi, \Psi) = e^\top P\dot{e} + \dot{e}^\top Pe + Tr\Big[\dot{\Phi}^\top N\Phi\Big] + Tr\big[\Phi^\top N\dot{\Phi}\big] \\ + Tr\Big[\dot{\Psi}^\top N\Psi\Big] + Tr\big[\Psi^\top N\dot{\Psi}\big]. \end{aligned} \tag{79}$$

By substituting (73) into the previous equation, and claiming the equality $PA_m + A_m^\top P = -Q$, it follows that,

$$\begin{aligned} \dot{V}_2 &= e^\top P\big(A_m e + G\Phi u + G\Psi r_m\big) + \big(A_m e + G\Phi u + G\Psi r_m\big)^\top Pe \\ &\quad + Tr\big[-ue^\top PSN\Phi\big] + Tr\Big[\Phi^\top N\big(-ue^\top PS\big)^\top\Big] \\ &\quad + Tr\big[-r_m e^\top PSN\Psi\big] + Tr\Big[\Psi^\top N\big(-r_m e^\top PS\big)^\top\Big] \\ &= -e^\top Qe + e^\top P\big(G\Phi u + G\Psi r_m\big) + \big(G\Phi u + G\Psi r_m\big)^\top Pe \\ &\quad + Tr\big[-ue^\top PSN\Phi\big] - Tr\big[\Phi^\top NS^\top Peu^\top\big] \\ &\quad + Tr\big[-r_m e^\top PSN\Psi\big] - Tr\big[\Psi^\top NS^\top Per_m^\top\big]. \end{aligned} \tag{80}$$

Let us consider that $G = SN$ is defined as in (71), while N is a Hermitian positive definite matrix such that $N^\top = N$, and also that $Tr(ab^\top A) = b^\top Aa$ holds, where $a, b \in \mathbb{R}^n$, and $A \in \mathbb{R}^{n\times n}$. Then, we get the following expression

$$\begin{aligned} \dot{V}_2 &= -e^\top Qe + e^\top P\big(G\Phi u + G\Psi r_m\big) + \big(G\Phi u + G\Psi r_m\big)^\top Pe \\ &\quad - e^\top PG\Phi u - u^\top\Phi^\top G^\top Pe - e^\top PG\Psi r_m - r_m^\top\Psi^\top G^\top Pe \\ &= -e^\top Qe. \end{aligned} \tag{81}$$

By applying Theorem 2.9 from [53], which is suitable for time-varying systems, we analyze the set:

$$\Lambda = \Big\{(e, \Phi, \Psi) \;\Big|\; \dot{V}_2(e, \Phi, \Psi) = 0\Big\}.$$

From (81), it follows that:

$$\dot{V}_2 = -e^\top Qe \Rightarrow \dot{V}_2 = 0 \Leftrightarrow e = 0. \tag{82}$$

Now, using $e = 0$ in (73), the parameter update laws reduce to:

$$\dot{\Phi} = -ue^\top PS = 0, \qquad \dot{\Psi} = -r_m e^\top PS = 0, \tag{83}$$

so we conclude that:

$$\dot{\Phi} \to 0, \qquad \dot{\Psi} \to 0. \tag{84}$$

However, this does not imply that $\Phi(t) \to 0$ or $\Psi(t) \to 0$ unless additional conditions are satisfied. In particular, parameter convergence requires the persistent excitation (PE) condition on the signals $u(t)$ and $r_m(t)$, which is not assumed in this work.

To proceed, observe that since $e = 0$, then $\dot{e} = 0$, which from (76) leads to:

$$\dot{u} - \dot{u}_m = 0. \tag{85}$$

Substituting (63) and (70) yields:

$$Au + Gr - A_m u_m - G_m r_m = 0. \tag{86}$$

By inserting the control law (72) into the equation above, we obtain:

$$Au + G(\Theta u + K r_m) - A_m u_m - G_m r_m = 0. \tag{87}$$

This expression is satisfied if and only if:

$$\Theta = G^{-1}(A_m - A), \qquad K = G^{-1} G_m, \tag{88}$$

which correspond to the nominal values Θ^*, K^* in (75). Therefore, we deduce:

$$\Phi = \Theta - \Theta^* = 0, \qquad \Psi = K - K^* = 0. \tag{89}$$

Thus, using the result above, we conclude that:

$$\Lambda = \left\{ (e, \Phi, \Psi) \;\middle|\; \dot{V}_2(e, \Phi, \Psi) = 0 \right\} \tag{90}$$

only contains the equilibrium point $e = 0_{3\times1}, \Phi = 0_{6\times6}, \Psi = 0_{6\times6}$. Therefore, the origin of the error system is globally asymptotically stable. □

Remark 4. Notice that in the adaptive law (73) it is only required to know the sign of the matrix of the unknown G in (70). Such a matrix can be easily known depending on the fully actuated hexa-rotor configuration. As the reader can observe, the proposed controllers only require knowing m and J, which are easily known parameters, [see controls (18), and (59)].

Remark 5. Notice that the reference model (64) together with control (63) make that the state u_m converges to u_d, the [Lemma 1]. Then, Theorem 3 demonstrates that the adaptive control law stabilizes the error $e = u - u_m$ to zero. These two facts imply that u converges to u_d at the end, as desired.

Remark 6. The adaptive control proposed in this paper deals with scenarios where the rotors' pose can have small variations in time (in-flight tilting, for instance), but always considering that the rotors' pose will have a constant value when the time tends to infinity. Then, as long as the assumption regarding the sign of the elements of matrix B does not change when the motors' pose changes, one can say that the control can work in case of variations of the rotors' pose. In case of changes in the rotors' pose, the varying angular parameters should keep the same sign values of matrix B with respect to the initial motors' pose configuration.

A diagram of the proposed adaptive controller is depicted in the *nonlinear adaptive controller* block of Figure 3.

4 | Simulations

This section presents the simulation results for the fully actuated hexa-rotor system (Σ, Π, Γ), stabilized by the proposed control algorithm, which integrates robust and adaptive controls (Equations 18, 59, 64, and 72). All simulations were carried out in MATLAB/Simulink R2023a on a standard PC (Intel i7 processor, 16 GB RAM), using the variable-step solver `ode45` with default tolerances. The simulations examine three distinct scenarios:

1. *Scenario 1*: Attitude tracking using the proposed adaptive controller.
2. *Scenario 2*: Path tracking using the proposed adaptive controller.
3. *Scenario 3*: Path tracking with direct passthrough of the position and attitude controllers to the control allocation and motor dynamics (*no adaptive controller involved*). This scenario is designed specifically for comparison purposes.

For all simulation scenarios, the parameters for the fully actuated hexa-rotor are consistent with those used in [42]. These parameters are detailed in Table 2. Moreover, we have intentionally included several uncertainties into the model: the discrepancy between the real and nominal parameter values is simulated by adding an ϵ value to the final allocation matrix, which will simulate a more realistic operating condition for the hexa-rotor. Using the previous α, β, λ parameters in Table 2, the motor rotation matrices $R^{\mathcal{B}}_{\mathcal{M}_i}$ for each motor are defined as:

$$R^{\mathcal{B}}_{\mathcal{M}_1}(26.5^\circ,\ 40^\circ,\ 0^\circ) = \begin{bmatrix} 0.7660 & 0.2868 & 0.5753 \\ 0 & 0.8949 & -0.4462 \\ -0.6428 & 0.3418 & 0.6856 \end{bmatrix}$$

$$R^{\mathcal{B}}_{\mathcal{M}_2}(-26.5^\circ,\ -40^\circ,\ 60^\circ) = \begin{bmatrix} 0.43830 & -0.6316 & -0.6740 \\ 0.6634 & 0.6959 & -0.2751 \\ 0.6428 & -0.3418 & 0.6856 \end{bmatrix}$$

$$R^{\mathcal{B}}_{\mathcal{M}_3}(26.5^\circ,\ 40^\circ,\ 120^\circ) = \begin{bmatrix} -0.3830 & -0.9184 & 0.0988 \\ 0.6634 & -0.1991 & 0.7213 \\ -0.6428 & 0.3418 & 0.6856 \end{bmatrix}$$

$$R^{\mathcal{B}}_{\mathcal{M}_4}(-26.5^\circ,\ -40^\circ, 180^\circ) = \begin{bmatrix} -0.7660 & -0.2868 & 0.5753 \\ 0 & -0.8949 & -0.4462 \\ 0.6428 & -0.3418 & 0.6856 \end{bmatrix}$$

$$R^{\mathcal{B}}_{\mathcal{M}_5}(26.5^\circ,\ 40^\circ,\ 240^\circ) = \begin{bmatrix} 0.3090 & 0.8684 & 0.3878 \\ -0.9511 & 0.2822 & 0.1260 \\ 0 & -0.4078 & 0.9131 \end{bmatrix}$$

$$R^{\mathcal{B}}_{\mathcal{M}_6}(-26.5^\circ,\ -40^\circ,\ 240^\circ) = \begin{bmatrix} -0.3830 & 0.6316 & -0.6740 \\ -0.6634 & -0.6959 & -0.2751 \\ -0.6428 & 0.3418 & 0.6856 \end{bmatrix}. \tag{91}$$

In addition to the system parameters, all simulation scenarios consider the following disturbances affecting the hexa-rotor attitude dynamics:

$$\Delta(t) = \begin{bmatrix} 0.2\cos(t) \\ 0.2\sin(t) \\ 0 \end{bmatrix}. \tag{92}$$

TABLE 2 | Physical parameters of the fully actuated hexa-rotor.

Parameter	Value	Parameter	Value
α_i	[26.5; −26.5; 26.5; −26.5; 26.5; −26.5] deg.	$J_m \in \mathbb{R}^{6\times6}$ (diagonal matrix)	6×10^{-6}kg m^2
β_i	[40; −40; 40; −40; 40; −40] deg.	$B_m \in \mathbb{R}^{6\times6}$ (diagonal matrix)	2×10^{-6}m^2/s
λ	60 deg.	$K_T \in \mathbb{R}^{6\times6}$ (diagonal matrix)	1.0
m	1.0 kg	k_f	3.13×10^{-8}
l	0.25 m	D	3×10^{-4}
J_{xx}	0.0820kg m^2	d	7.5×10^{-7}
J_{yy}	0.0845kg m^2		
J_{zz}	0.1377kg m^2		

TABLE 3 | The initial conditions for Scenario 1.

Parameter	Value	Parameter	Value
$\phi(0)$	0 deg	$x(0)$	0 m
$\theta(0)$	0 deg	$y(0)$	0 m
$\psi(0)$	0 deg	$z(0)$	0 m
$\dot{\phi}(0)$	0 deg/s	$\dot{x}(0)$	0 m/s
$\dot{\theta}(0)$	0 deg/s	$\dot{y}(0)$	0 m/s
$\dot{\psi}(0)$	0 deg/s	$\dot{z}(0)$	0 m/s

Disturbances are added to prove that the proposed control algorithm is robust.

4.1 | Scenario 1: Attitude Tracking

In this scenario, the attitude dynamics is verified to converge to arbitrary desired trajectories. It is also intended to show that the rotations do not affect the position dynamics due to the attitude tracking. The initial conditions for this simulation are shown in Table 3. Notice that the simulation begins with the hexa-rotor flying at 5 m of altitude. During the simulation, the hexa-rotor should follow the desired trajectories:

$$\begin{bmatrix}\phi_d\\ \theta_d\\ \psi_d\end{bmatrix} = \begin{bmatrix}10\sin(0.2t)\ \text{deg}\\ 15\sin(0.2t)\ \text{deg}\\ 0\ \text{deg}\end{bmatrix}, \quad \begin{bmatrix}x_d\\ y_d\\ z_d\end{bmatrix} = \begin{bmatrix}0\ \text{m}\\ 0\ \text{m}\\ 5\ \text{m}\end{bmatrix}, \tag{93}$$

where t is the simulation time. Figure 4 depicts the simulation's results for the attitude and position states, and Figure 5 shows the controls and the spin of the six motors. The hexa-rotor is tracking the desired trajectories and maintaining a stable position. Besides the changes in the hexa-rotor's attitude, the hexa-rotor suffers minimal displacements in the position states since the changes in (ϕ, θ) do not involve a position displacement, as expected in standard multi-rotors. With these results, it is clear that our control preserves the full actuation of the hexa-rotor, showing that it performs attitude commands without affecting the position states.

4.2 | Scenario 2: Path Tracking

This scenario shows the convergence of position states to the given desired trajectories. We verify the full actuation by observing that the attitude states do not present significant changes despite the position displacements in the fully actuated hexa-rotor. The simulation begins with the initial conditions shown in Table 4.

The path-tracking simulation consists of a spiral trajectory along the y-axis. The desired trajectory for this motion is mathematically defined as:

$$\begin{bmatrix}x_d\\ y_d\\ z_d\end{bmatrix} = \begin{bmatrix}5\cos\left(\frac{\pi}{10}t\right)\\ \frac{1}{15}t\\ 5\sin\left(\frac{\pi}{10}t\right)\end{bmatrix}\text{m}. \tag{94}$$

This trajectory challenges the hexa-rotor's ability to perform simultaneous position and attitude control while maintaining robustness under the uncertainties and external disturbances considered in the simulation. The desired trajectories for the attitude states are set to 0 degrees.

Figure 6 shows the results for the attitude and position states, and Figure 7 depicts the results of the controls and motors' spin. These figures show that the attitude states have minimal changes while the hexa-rotor displaces along the circumference. The hexa-rotor adapts its control gains during the initial transient phase using the proposed adaptive algorithm. After that, the hexa-rotor advances steadily along the y-axis at a constant speed while performing circular maneuvers in the x-z plane.

4.3 | Scenario 3: Path Tracking Without the Proposed Adaptive Controller

To underscore the significance of the proposed adaptive controller, a third scenario is introduced in which no adaptive controller is employed. In this case, the position and attitude controllers directly interface with the control allocation and motor dynamics. The simulation conditions are identical to those in the previous scenario, with the initial conditions provided in Table 4. The position and attitude states for this scenario are illustrated in Figure 8. As shown, the primary controller struggles to guide the aerial vehicle effectively along the desired trajectory, primarily due to its lack of robustness against parameter uncertainties and external disturbances.

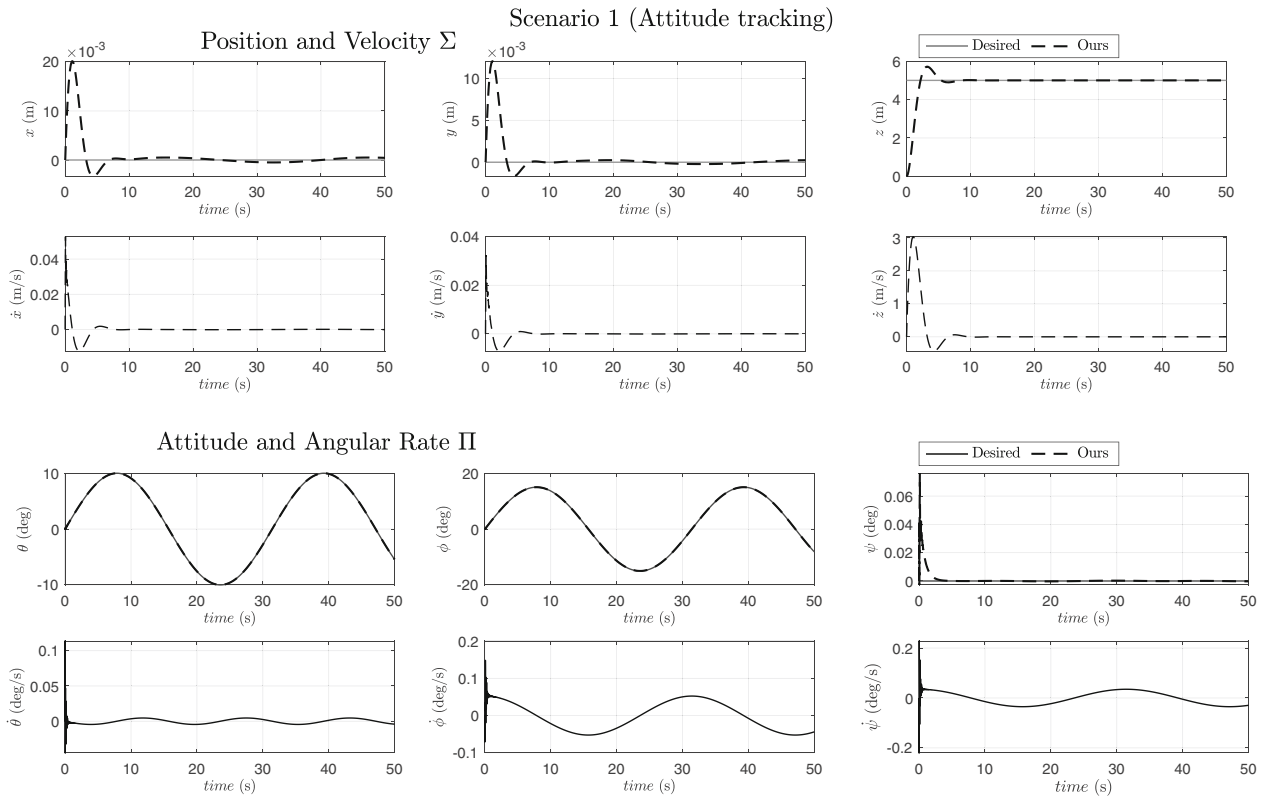

FIGURE 4 | This figure shows the simulation results of Scenario 1 (attitude tracking). The attitude tracking consists of desired signals given by (93). In the attitude plots (θ, ϕ, and ψ), the hexa-rotor satisfactorily tracks the desired values on each axis. Moreover, the position and velocity plots show no significant displacement; the small variations are due to exogenous disturbances and can be minimized by choosing higher gains.

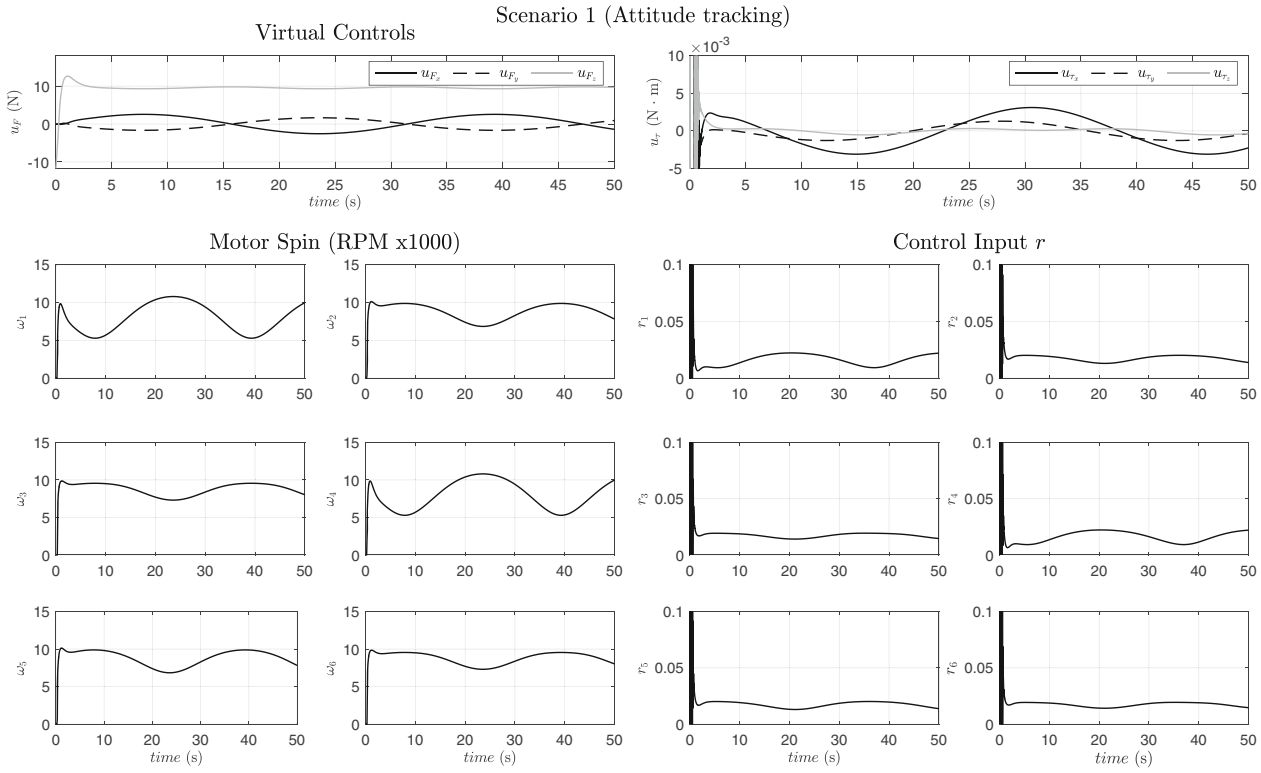

FIGURE 5 | Control response during the simulation of Scenario 1. In this figure, the virtual control response (59) and (18) (top graphs) are depicted. Also, the six right-hand side graphs depict the adaptive and robust control outputs (72). Finally, the left-hand side six graphs show the resultant motor spin (v) that controls the hexa-rotor.

Moreover, the attitude states exhibit oscillatory behavior, particularly after 40 s, despite maintaining a relatively fixed position. This indicates instability that can compromise performance. Additionally, Figure 9 reveals that the control signals exhibit significant noise, a phenomenon that could pose serious challenges during real-world flight operations.

A notable comparison can also be made between the motor spin dynamics in the proposed adaptive control and the case where only position and attitude controllers are used, as shown in Figures 7 and 9. The proposed adaptive controller achieves smoother and more consistent performance, while the primary control generates a highly noisy response, further emphasizing the effectiveness of the adaptive strategy.

TABLE 4 | The initial conditions for Scenarios 2 and 3.

Parameter	Value	Parameter	Value
$\phi(0)$	0 deg	$x(0)$	0 m
$\theta(0)$	0 deg	$y(0)$	0 m
$\psi(0)$	0 deg	$z(0)$	0 m
$\dot{\phi}(0)$	0 deg/s	$\dot{x}(0)$	0 m/s
$\dot{\theta}(0)$	0 deg/s	$\dot{y}(0)$	0 m/s
$\dot{\psi}(0)$	0 deg/s	$\dot{z}(0)$	0 m/s

4.4 | Performance Evaluation

After simulating Scenarios 2 and 3, with and without the proposed adaptive controller, respectively, different errors are calculated based on the performance evaluation conducted in [54]. The aim is to quantitatively evaluate the performance of the results in Scenario 2, where the adaptive control approach is used, and compare it to the results in Scenario 3, where only position and attitude controllers are used without adaptive control. The three calculated errors are the Integral Squared Error (ISE), the Integral of Absolute Error (IAE), and the Integral of Time-weighted Absolute Error (ITAE) using the following equations:

$$\text{ISE} = \int_0^\infty e^2(t)dt, \quad \text{IAE} = \int_0^\infty |e^2(t)|dt,$$
$$\text{ITAE} = \int_0^\infty t|e^2(t)|dt. \tag{95}$$

These errors are computed for the position and attitude states. The results can be seen in Table 5; it is clear that in most of the cases, the proposed control approach performs better than only using the position and attitude controller. The ITAE results reveal a significant disparity in errors, highlighting the superior long-term performance of the adaptive control approach compared to the nonadaptive controller. As expected, the system

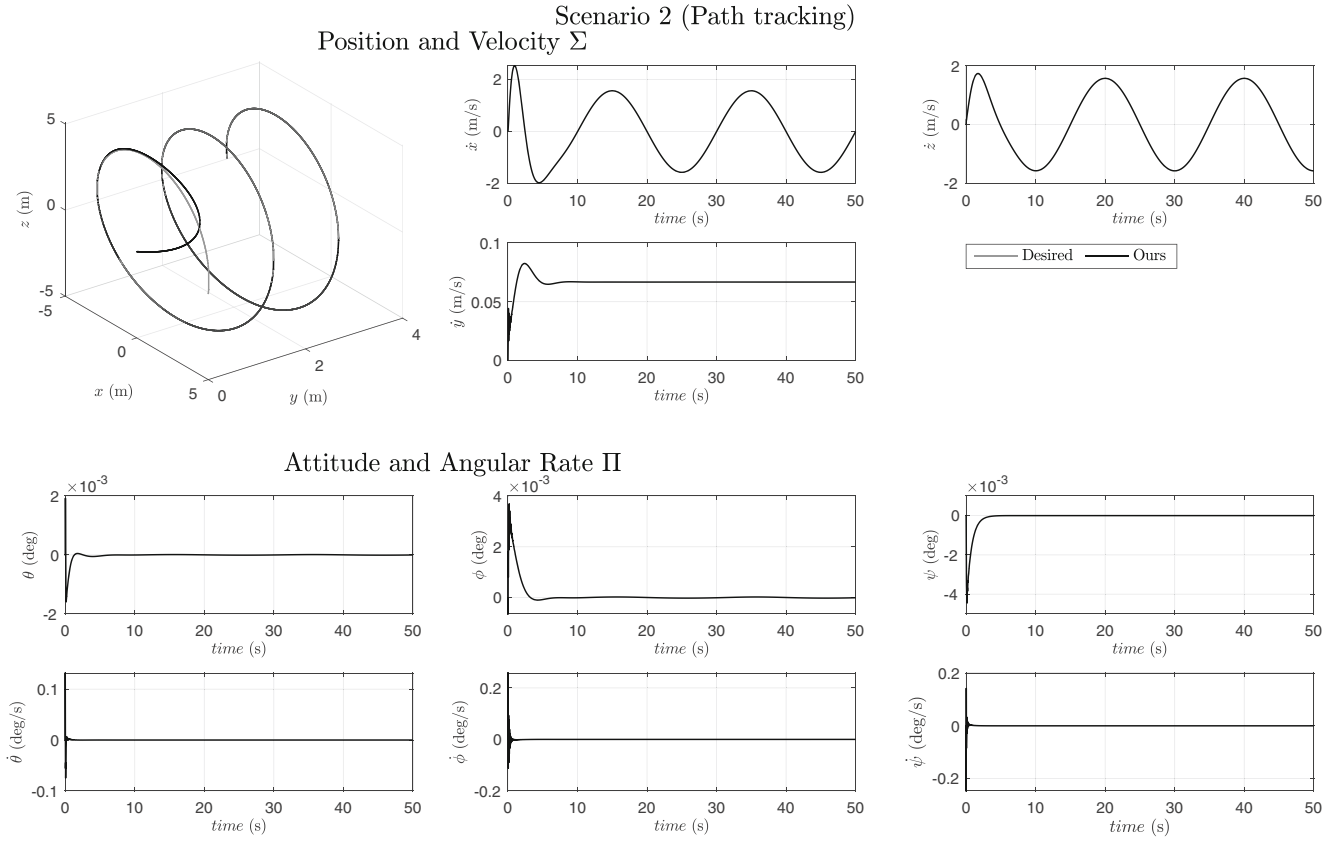

FIGURE 6 | The path-tracking simulation illustrates a spiral trajectory along the y-axis. The hexa-rotor advances along the y-axis at a constant speed while performing circular maneuvers in the x-z plane. The simulation results demonstrate that the proposed robust control system achieves smooth state responses, maintaining minimal errors between the actual and desired trajectories. Notably, the hexa-rotor's attitude experiences close null deviations despite the complexity of the longitudinal motion. The proposed controller ensures stable performance even in the presence of model uncertainties and external disturbances.

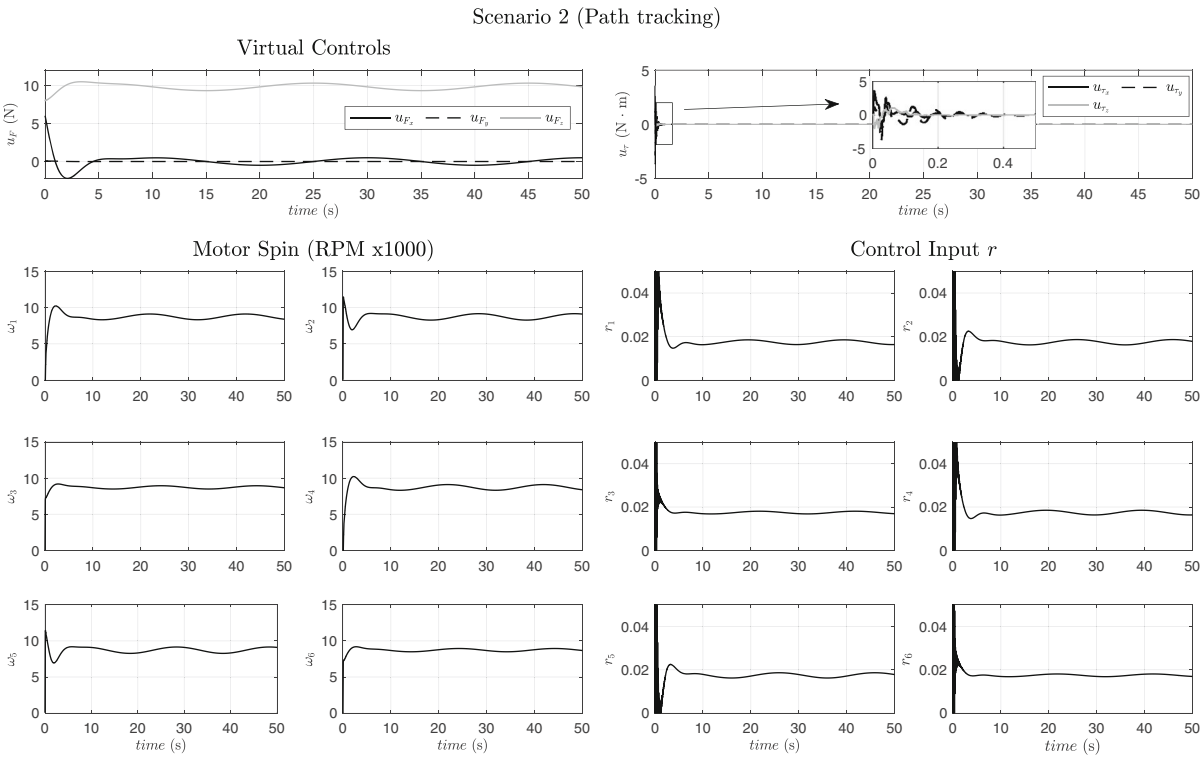

FIGURE 7 | Control results during the simulation of Scenario 2 *with the proposed adaptive controller*. The upper two graphs illustrate the virtual control outputs, u_F and u_τ, derived from (59) and (18), respectively. The six right-hand side graphs display the adaptive control inputs, r_1 to r_6, as defined by (72). Lastly, the six left-hand side graphs present the resultant motor spin velocities, ω_1 to ω_6, which drive the hexa-rotor. These results demonstrate the system's ability to maintain smooth and stable control responses under the proposed adaptive framework.

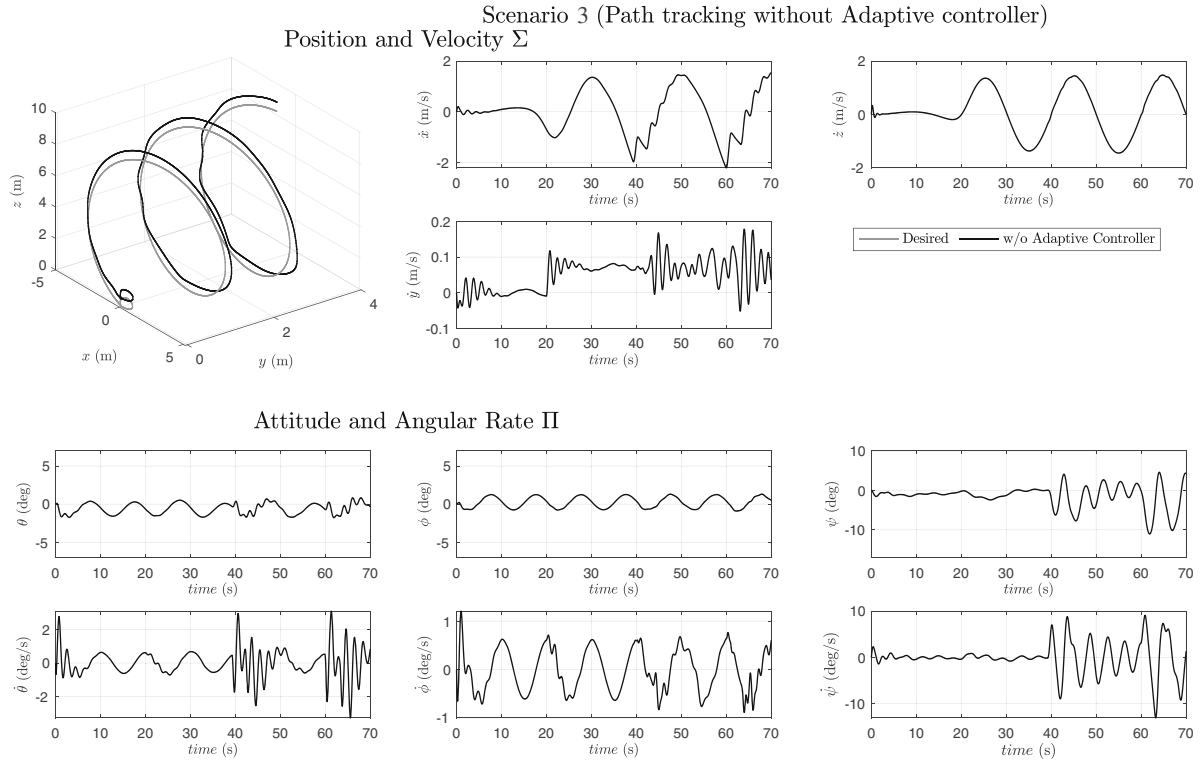

FIGURE 8 | Simulation results for *Scenario 3*: Path tracking *without* the Proposed Adaptive Controller, where only the main position and attitude controllers are employed. While the state response initially follows the desired trajectory, significant position errors arise as the hexa-rotor navigates the circular path. Additionally, during hover flight, the hexa-rotor's attitude exhibits oscillatory noise, and during path-following maneuvers, the attitude control performance is noticeably suboptimal. These issues are attributed to the lack of robustness in the main controller, which is unable to compensate for external disturbances and parameter uncertainties, ultimately failing to stabilize the system effectively.

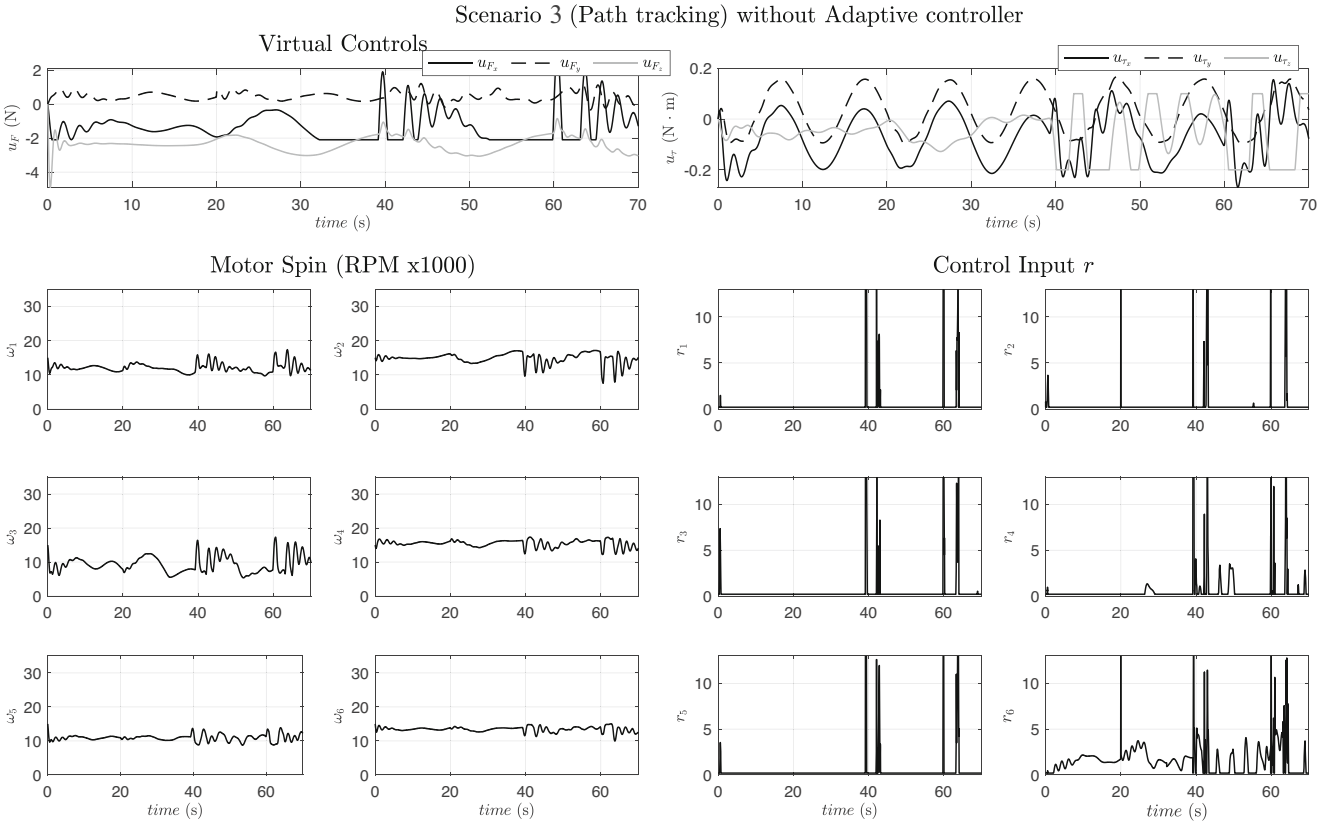

FIGURE 9 | Control inputs and angular motor velocities during the simulation of *Scenario 3*: path tracking *without* the proposed adaptive controller. The virtual control outputs, derived from (18) and (59), are shown in the upper two graphs. The six bottom graphs illustrate the resultant motor spin velocities that drive the fully actuated hexa-rotor. As observed, both the virtual controls (u_F and u_τ) and the motor spins exhibit significant noise and instability, especially under the influence of external disturbances and parameter uncertainties. This behavior contrasts sharply with the smoother and more consistent response achieved by the proposed robust adaptive control.

TABLE 5 | Integral error results from simulations in Scenario 2 (adaptive) and Scenario 3 (nonadaptive).

State	ISE		IAE		ITAE	
	Nonadaptive	**Adaptive**	**Nonadaptive**	**Adaptive**	**Nonadaptive**	**Adaptive**
x	29.1817	**22.4174**	28.6443	**7.4563**	1552.3	**10.8819**
y	0.8923	**0.013**	4.2297	**0.0683**	248.5050	**0.2087**
z	0.6179	**0.6976**	6.9033	**1.5251**	280.0237	**3.7923**
θ	72.4930	**0.0000**	60.3110	**0.0764**	2334.5	**0.9384**
ϕ	46.5219	**0.0004**	52.8193	**0.2777**	2152.2	**2.2424**
ψ	5392.3557	**0.0004**	404.3903	**1929**	23570.3	**0.1725**

Note: The bold values under the Adaptive columns highlight an error reduction compared to the values under the Nonadaptive column.

accumulates higher errors over time for the approach without adaptive control.

5 | Conclusions

This paper investigates the modeling and control of the fully actuated hexa-rotor. This kind of aerial vehicle configuration has the principal characteristic of decoupling position and attitude dynamics. However, it is observed that such decoupling between the position and attitude states has a limit, which means that it is impossible to move at high speed without changing the attitude of the UAV, and the same is true with high angular values.

This work's main contribution is designing a robust and adaptive controller to stabilize a fully actuated hexa-rotor UAV for which only the configuration—the direction of the rotors' orientations—is known under exogenous signals and parameter uncertainties. First, the robust virtual attitude and position control are designed to reference the six motor angular velocities. Next, an adaptive control approach is developed to allow the hexa-rotor to modify its motors' angular velocities, compensating

for the parameter uncertainties to produce the virtual reference controls.

Three different simulation scenarios were performed with the parameters' angular values as unknown, and external disturbances were included. In these simulation scenarios, it was possible to evaluate and compare the control performance. The first two simulations showed that the proposed approach could independently control the fully actuated hexa-rotor in position and angular displacements. The third simulation compared the performance between our proposed adaptive controller and the implementation of only the position and attitude controller, showing the robustness of the proposed control.

As further work, we intend to construct a small, fully actuated hexa-rotor prototype to implement the proposed control scheme.

Funding

The authors have nothing to report.

Conflicts of Interest

The authors declare no conflicts of interest.

Data Availability Statement

The data that support the findings of this study are available from the corresponding author upon reasonable request.

Endnotes

[1]Equation (13) will be used in step two of our control law.

[2]It can be demonstrated that such an assumption is easily achieved for various configurations of the fully actuated hexa-rotor.

References

1. W. Giernacki, M. Skwierczyński, W. Witwicki, P. Wroński, and P. Kozierski, "Crazyflie 2.0 Quadrotor as a Platform for Research and Education in Robotics and Control Engineering," in *2017 22nd International Conference on Methods and Models in Automation and Robotics (MMAR)* (IEEE, 2017), 37–42, https://doi.org/10.1109/MMAR.2017.8046794.

2. K. N. McGuire, C. D. Wagter, K. Tuyls, H. J. Kappen, and D. G. C. H. E. Croon, "Minimal Navigation Solution for a Swarm of Tiny Flying Robots to Explore an Unknown Environment," *Science Robotics* 4, no. 35 (2019): eaaw9710, https://doi.org/10.1126/scirobotics.aaw9710.

3. G. Freire and R. Cota, "Capture of Images in Inaccessible Areas in an Underground Mine Using an Unmanned Aerial Vehicle," in *Proceedings of the First International Conference on Underground Mining Technology*, ed. M. Hudyma and Y. Potvin (Australian Centre for Geomechanics, 2017).

4. J. G. R. Iii, R. E. Sherrill, A. Schang, et al., "Distributed Subterranean Exploration and Mapping With Teams of UAVs," in *Ground/Air Multisensor Interoperability, Integration, and Networking for Persistent ISR VIII*, vol. 10190, ed. T. Pham and M. A. Kolodny (International Society for Optics and Photonics. SPIE, 2017), 285–301.

5. M. D. Hua, T. Hamel, P. Morin, and C. Samson, "Introduction to Feedback Control of Underactuated VTOLvehicles: A Review of Basic Control Design Ideas and Principles," *IEEE Control Systems Magazine* 33, no. 1 (2013): 61–75, https://doi.org/10.1109/MCS.2012.2225931.

6. F. Ruffier and N. Franceschini, "Optic Flow Regulation: The Key to Aircraft Automatic Guidance," *Robotics and Autonomous Systems* 50, no. 4 (2005): 177–194 Biomimetic Robotics, https://doi.org/10.1016/j.robot.2004.09.016.

7. A. Argyros, D. Tsakiris, and C. Groyer, "Biomimetic Centering Behavior [Mobile Robots With Panoramic Sensors]," *IEEE Robotics and Automation Magazine* 11, no. 4 (2004): 21–30, https://doi.org/10.1109/MRA.2004.1371612.

8. G. Ramírez, R. Verdín, and G. Flores, "Real-Time Mapping for Teleoperation Systems in VR of Unmanned Aerial Vehicles," in *Proceedings of the 2024 International Conference on Unmanned Aircraft Systems (ICUAS)* (IEEE, 2024), 1002–1009, https://doi.org/10.1109/ICUAS60882.2024.10556921.

9. G. Flores, "Longitudinal Modeling and Control for the Convertible Unmanned Aerial Vehicle: Theory and Experiments," *ISA Transactions* 122 (2022): 312–335, https://doi.org/10.1016/j.isatra.2021.04.043.

10. E. Vega, R. Verdín, N. Aldana, and G. Flores, "Barrier Lyapunov Function-Based Control for Position-Based Visual Servoing of Fully Actuated UAVs Within PX4," in *Proceedings of the 2025 International Conference on Unmanned Aircraft Systems (ICUAS)* (IEEE, 2025), 124–131, https://doi.org/10.1109/ICUAS65942.2025.11007906.

11. G. Flores and M. W. Spong, "The Soft-PVTOL: Modeling and Control," *Robotics and Autonomous Systems* 187 (2025): 104925, https://doi.org/10.1016/j.robot.2025.104925.

12. R. Rashad, J. Goerres, R. Aarts, J. B. C. Engelen, and S. Stramigioli, "Fully Actuated Multirotor UAVs: A Literature Review," *IEEE Robotics and Automation Magazine* 27, no. 3 (2020): 97–107, https://doi.org/10.1109/MRA.2019.2955964.

13. A. Garofano-Soldado, A. Gonzalez-Morgado, G. Heredia, and A. Ollero, "Assessment and Modeling of the Aerodynamic Ground Effect of a Fully-Actuated Hexarotor With Tilted Propellers," *IEEE Robotics and Automation Letters* 9, no. 2 (2024): 1907–1914, https://doi.org/10.1109/LRA.2024.3350975.

14. Y. Wang, X. You, and M. Baghdadi, "Non-Linear Model Predictive Control of a Tilt-Rotor Quadcopter for Control Allocation and Path Following," in *(IEEE) 2024 International Conference on Global Aeronautical Engineering and Satellite Technology (GAST)* (IEEE, 2024), 1–6, https://doi.org/10.1109/GAST60528.2024.10520761.

15. H. Romero, S. Salazar, and R. Lozano, "Real-Time Stabilization of an Eight-Rotor UAV Using Optical Flow," *IEEE Transactions on Robotics* 25, no. 4 (2009): 809–817, https://doi.org/10.1109/TRO.2009.2018972.

16. S. Rajappa, M. Ryll, H. H. Bülthoff, and A. Franchi, "Modeling, Control and Design Optimization for a Fully-Actuated Hexarotor Aerial Vehicle With Tilted Propellers," in *2015 IEEE International Conference on Robotics and Automation (ICRA)* (IEEE, 2015), 4006–4013, https://doi.org/10.1109/ICRA.2015.7139759.

17. M. Tognon and A. Franchi, "Omnidirectional Aerial Vehicles With Unidirectional Thrusters: Theory, Optimal Design, and Control," *IEEE Robotics and Automation Letters* 3, no. 3 (2018): 2277–2282, https://doi.org/10.1109/LRA.2018.2802544.

18. T. Amandyk, G. Igor, G. Pavel, and K. Moldir, "Design and Control System of a Fully Actuated UAV for Mines Monitoring," in *Advances in Asian Mechanism and Machine Science*, ed. A. Tuleshov, A. Jomartov, and M. Ceccarelli (Springer Nature Switzerland, 2024), 267–279.

19. J. X. J. Bannwarth, S. Kazemi, and K. Stol, "Frequency-Dependent H∞ Control for Wind Disturbance Rejection of a Fully Actuated UAV," *Robotica* 42, no. 6 (2024): 1781–1795, https://doi.org/10.1017/S0263574724000523.

20. J. Jaramillo, K. Wilcher, T. Yucelen, and M. Pakmehr, "Development of a Model Reference Adaptive Control Architecture in a Hexarotor Simulation Environment," in *American Institute of Aeronautics and Astronautics (AIAA)* (AIAA, 2024), https://doi.org/10.2514/6.2024-0757.

21. Z. Li, Y. Yang, and Z. Li, "Nonlinear Generalized Predictive Control for a Novel Thrust-Vectoring Hexarotor Using Super-Twisting ESO," in

IECON 2024-50th Annual Conference of the IEEE Industrial Electronics Society (IEEE, 2024), 1–6.

22. K. Cao, H. Hu, H. Cheng, X. Wang, H. Wu, and J. Gu, "Fault-Tolerant Control of Hexa-Rotor Unmanned Aerial Vehicles Based on Backstepping," in *Advanced Control and Intelligent Computing Applications*, ed. C. Peng, Y. Wang, Y. Guan, Q. Sun, Z. Chen, and Y. Zhang (Springer Nature, 2025), 3–16.

23. W. Park, X. Wu, D. Lee, and S. J. Lee, "Design, Modeling and Control of a Top-Loading Fully-Actuated Cargo Transportation Multirotor," *IEEE Robotics and Automation Letters* 8, no. 9 (2023): 5807–5814, https://doi.org/10.1109/LRA.2023.3300248.

24. J. Lee, K. Leang, and W. Yim, "Design and Control of a Fully-Actuated Hexrotor for Aerial Manipulation Applications," *Journal of Mechanisms and Robotics* 10 (2018): 041007, https://doi.org/10.1115/1.4039854.

25. G. Jiang and R. Voyles, "Hexrotor UAV Platform Enabling Dextrous Interaction With Structures-Flight Test," in *Proceedings of the 2013 IEEE International Symposium on Safety, Security, and Rescue Robotics (SSRR)* (IEEE, 2013), 1–6.

26. Y. Tadokoro, T. Ibuki, and M. Sampei, "Maneuverability Analysis of a Fully-Actuated Hexrotor UAV Considering Tilt Angles and Arrangement of Rotors," *IFAC-PapersOnLine* 50, no. 1 (2017): 8981–8986, https://doi.org/10.1016/j.ifacol.2017.08.1325.

27. M. Ryll, D. Bicego, and A. Franchi, "Modeling and Control of FAST-Hex: A Fully-Actuated by Synchronized-Tilting Hexarotor," in *Proceedings of the 2016 IEEE/RSJ International Conference on Intelligent Robots and Systems (IROS)* (2016), 1689–1694, https://doi.org/10.1109/IROS.2016.7759271.

28. M. Ryll, D. Bicego, M. Giurato, M. Lovera, and A. Franchi, "FAST-Hex – A Morphing Hexarotor: Design, Mechanical Implementation, Control and Experimental Validation," *IEEE/ASME Transactions on Mechatronics* 27, no. 3 (2021), https://doi.org/10.1109/TMECH.2021.3099197.

29. J. M. Arizaga, A. Miranda-Moya, H. Castañeda, and P. Castillo, "Observer-Based Adaptive Control for Slung Payload Stabilization With a Fully-Actuated Multirotor UAV," *ISA Transactions* 147 (2024): 109–117, https://doi.org/10.1016/j.isatra.2024.02.015.

30. D. Lee and H. J. Kim, "Saturated RISE Control for Considering Rotor Thrust Saturation of Fully Actuated Multirotor," in *International Conference on Unmanned Aircraft Systems* (IEEE, 2024), 39–44, https://doi.org/10.1109/ICUAS60882.2024.10557062.

31. C. Wang, R. Jiao, and J. Zhang, "Nonlinear Observer-Based Impedance Control of a Fully-Actuated Hexarotor for Accurate Aerial Physical Interaction," *Industrial Robot: The International Journal of Robotics Research and Application* 51, no. 4 (2024): 683–695, https://doi.org/10.1108/IR-11-2023-0268.

32. M. Perin, M. Bertoni, G. Michieletto, R. Oboe, and A. Cenedese, "Trajectory Tracking for Tilted Hexarotors With Concurrent Attitude Regulation," in *Proceedings of the 2024 American Control Conference (ACC)* (IEEE, 2024), 1550–1555, https://doi.org/10.23919/ACC60939.2024.10644887.

33. M. Ordaz, O. Santos Sánchez, P. Ordaz, H. Trejo, and O. Pérez, "Robust Linear Discrete Control for a Hexacopter: Experimental Results," *International Journal of Combinatorial Optimization Problems and Informatics* 15 (2024): 183–204, https://doi.org/10.61467/2007.1558.2024.v15i3.423.

34. G. He, Y. Jangir, J. Geng, M. Mousaei, D. Bai, and S. Scherer, "Image-Based Visual Servo Control for Aerial Manipulation Using a Fully-Actuated UAV," in *2023 IEEE/RSJ International Conference on Intelligent Robots and Systems (IROS)* (2023), 5042–5049, https://dois.org/10.1109/IROS55552.2023.10342145.

35. G. Pimentel, M. Santos, J. Lima, P. Mercorelli, and F. Fernandes, "An Over-Actuated Hexacopter Tilt-Rotor UAV Prototype for Agriculture of Precision: Modeling and Control," *Sensors* 25 (2025): 479, https://doi.org/10.3390/s25020479.

36. Z. Li, H. Wang, X. Zhang, Y. Liu, X. Zhang, and Y. Zhuang, "Nonlinear Control of a Fully-Actuated Hexacopter With a Cable-Suspended Load," in *Proceedings of the 2024 14th Asian Control Conference (ASCC)* (IEEE, 2024), 2340–2345.

37. C. Yao, J. Krieglstein, and K. Janschek, "Modeling and Sliding Mode Control of a Fully-Actuated Multirotor With Tilted Propellers," *IFAC-PapersOnLine* 51, no. 22 (2018): 115–120, https://doi.org/10.1016/j.ifacol.2018.11.527.

38. B. Convens, K. Merckaert, M. M. Nicotra, R. Naldi, and E. Garone, "Control of Fully Actuated Unmanned Aerial Vehicles With Actuator Saturation," *IFAC-PapersOnLine* 50, no. 1 (2017): 12715–12720, https://doi.org/10.1016/j.ifacol.2017.08.1823.

39. N. P. Nguyen, W. Kim, and J. Moon, "Super-Twisting Observer-Based Sliding Mode Control With Fuzzy Variable Gains and Its Applications to Fully-Actuated Hexarotors," *Journal of the Franklin Institute* 356, no. 8 (2019): 4270–4303, https://doi.org/10.1016/j.jfranklin.2019.03.005.

40. R. Rashad, J. B. C. Engelen, and S. Stramigioli, "Energy Tank-Based Wrench/Impedance Control of a Fully-Actuated Hexarotor: A Geometric Port-Hamiltonian Approach," in *Proceedings of the 2019 International Conference on Robotics and Automation (ICRA)* (IEEE, 2019), 6418–6424, https://doi.org/10.1109/ICRA.2019.8793939.

41. S. Rajappa, H. H. Bülthoff, M. Odelga, and P. Stegagno, "A Control Architecture for Physical Human-UAV Interaction With a Fully Actuated Hexarotor," in *Proceedings of the 2017 IEEE/RSJ International Conference on Intelligent Robots and Systems (IROS)* (IEEE, 2017), 4618–4625, https://doi.org/10.1109/IROS.2017.8206332.

42. D. Bicego, J. Mazzetto, R. Carli, M. Farina, and A. Franchi, "Nonlinear Model Predictive Control With Enhanced Actuator Model for Multi-Rotor Aerial Vehicles With Generic Designs," *Journal of Intelligent & Robotic Systems* 100, no. 3 (2020): 1213–1247, https://doi.org/10.1007/s10846-020-01250-9.

43. D. Shawky, C. Yao, and K. Janschek, "Nonlinear Model Predictive Control for Trajectory Tracking of a Hexarotor With Actively Tiltable Propellers," in *Proceedings of the 2021 7th International Conference on Automation, Robotics and Applications (ICARA)* (IEEE, 2021), 128–134, https://doi.org/10.1109/ICARA51699.2021.9376523.

44. C. Wang, Y. Xia, X. Kong, and T. Wang, "Attitude Control of Underactuated Quadrotor UAV Based on Improved ADRC," in *Proceedings of the 2023 2nd Conference on Fully Actuated System Theory and Applications* (IEEE, 2023), 699–704, https://doi.org/10.1109/CFASTA57821.2023.10243364.

45. F. Amiri and S. Khorashadizadeh, "Adaptive Control of a Class of Uncertain Nonlinear Systems Using Brain Emotional Learning and Legendre Polynomials," *Transactions of the Institute of Measurement and Control* 46, no. 9 (2024): 1667–1679, https://doi.org/10.1177/01423312231203270.

46. R. Zarei and S. Khorashadizadeh, "Direct Adaptive Model-Free Control of a Class of Uncertain Nonlinear Systems Using Legendre Polynomials," *Transactions of the Institute of Measurement and Control* 41, no. 11 (2019): 3081–3091, https://doi.org/10.1177/0142331218821408.

47. T. A. H. Alqutami, M. W. Dunnigan, and Y. Petillot, "Modeling and Motion Control of a Fully Actuated Multirotor for Aerial Manipulation Using PX4 and ROS2," in *Proceedings of the 2024 9th International Conference on Mechatronics Engineering (ICOM)* (IEEE, 2024), 396–401, https://doi.org/10.1109/ICOM61675.2024.10652521.

48. S. Al-zubaidi and K. Stol, "Design Optimisation of Fully Actuated UAVs Using Hybrid Optimisation," *Journal of Intelligent & Robotic Systems* 111, no. 1 (2025): 19, https://doi.org/10.1007/s10846-025-02227-2.

49. Y. Naoki, S. Nagai, and H. Fujimoto, "Mode-Switching Algorithm to Improve Variable-Pitch-Propeller Thrust Generation for Drones Under

Motor Current Limitation," *IEEE/ASME Transactions on Mechatronics* 28, no. 4 (2023): 2003–2011, https://doi.org/10.1109/TMECH.2023.3275618.

50. R. Gasch and J. Twele, *Wind Power Plants* (Springer, 2007).

51. F. Bullo and A. D. Lewis, *Geometric Control of Mechanical Systems* (Springer-Verlag New York, 2005).

52. N. J. Higham, "The Matrix Sign Decomposition and Its Relation to the Polar Decomposition," *Linear Algebra and its Applications* 212 (1994): 3–20, https://doi.org/10.1016/0024-3795(94)90393-X.

53. K. S. Narendra and A. M. Annaswamy, *Stable Adaptive Systems* (Dover Books, 2005).

54. A. Izadbakhsh, A. Deylami, and S. Khorashadizadeh, "Superiority of q-Chlodowsky Operators Versus Fuzzy Systems and Neural Networks: Application to Adaptive Impedance Control of Electrical Manipulators," *Expert Systems with Applications* 209 (2022): 118249, https://doi.org/10.1016/j.eswa.2022.118249.